Molecular Microbiology (2016) 99(1), 151–171 ■
doi:10.1111/mmi.13222
First published online 20 October 2015

Proteomic analysis of the *Simkania*-containing vacuole: the central role of retrograde transport

Jo-Ana Herweg,[1] Valérie Pons,[2] Dörte Becher,[3] Michael Hecker,[4] Georg Krohne,[5] Julien Barbier,[2] Hilmar Berger,[6] Thomas Rudel[1]* and Adrian Mehlitz[1,6]

[1]*Department of Microbiology and* [5]*Division of Electron Microscopy, University of Würzburg, Biocenter, Am Hubland, D-97074, Würzburg, Germany.*

[2]*DSV, iBiTec-S, LabEx LERMIT, CEA, F-91191, Gif sur Yvette, France.*

[3]*Department of Microbial Proteomics and* [4]*Microbial Physiology/Molecular Biology, University of Greifswald, Institute of Microbiology, Friedrich-Ludwig-Jahn-Straße 15, D-17487, Greifswald, Germany.*

[6]*Department of Molecular Biology, Max-Planck-Institute for Infection Biology, Charitéplatz 1, D-10117, Berlin, Germany.*

Summary

Simkania negevensis **is an obligate intracellular bacterial pathogen that grows in amoeba or human cells within a membrane-bound vacuole forming endoplasmic reticulum (ER) contact sites. The membrane of this *Simkania*-containing vacuole (SnCV) is a critical host–pathogen interface whose origin and molecular interactions with cellular organelles remain poorly defined. We performed proteomic analysis of purified ER-SnCV-membranes using label free LC-MS^2 to define the pathogen-containing organelle composition. Of the 1,178 proteins of human and 302 proteins of *Simkania* origin identified by this strategy, 51 host cell proteins were enriched or depleted by infection and 57 proteins were associated with host endosomal transport pathways. Chemical inhibitors that selectively interfere with trafficking at the early endosome-to-trans-Golgi network (TGN) interface (retrograde transport) affected SnCV formation, morphology and lipid transport. Our data demonstrate that *Simkania* exploits early endosome-to-TGN transport for nutrient acquisition and growth.**

Accepted 12 September, 2015. *For correspondence. E-mail thomas.rudel@biozentrum.uni-wuerzburg.de; Tel. +49 931 31 84401; Fax +49 931 31 84402.

Introduction

The obligate intracellular, Gram-negative bacterium *Simkania negevensis* (*Sn*) belongs to the family *Simkaniaceae* in the order *Chlamydiales* (Everett *et al*., 1999; Kahane *et al*., 2007). The genome of *Sn* is approximately 2.5 Mbp in size and thus two to three times larger than the genome of *Chlamydia* (Collingro *et al*., 2011). *Chlamydiae* are found as symbionts and pathogens in a wide range of eukaryotes, including protists, invertebrates and vertebrates (Subtil *et al*., 2014). *Sn* is able to replicate in amoebae, human and simian epithelial cells and macrophages (Kahane *et al*., 1993; 2007) and has been associated with infections of the upper respiratory tract in infants and adults (Lieberman *et al*., 1997; Kahane *et al*., 1998; Horn, 2008; Lamoth and Greub, 2010). Infections with the two closely related human pathogenic bacteria *Chlamydia pneumoniae* and *Chlamydia psittaci* can cause community acquired or animal transmitted pneumonia, chronic bronchitis and chronic asthma (Hughes *et al*., 1997; Hahn and McDonald, 1998; Harkinezhad *et al*., 2009).

Similar to *Chlamydia*, *Sn* undergoes a unique developmental cycle during intracellular replication. Infection is initiated by entry of an electron dense elementary body (EB) into the host cell. Inside of a membrane-bound compartment, termed inclusion, EBs differentiate into reticulate bodies (RBs) within a short period of time. RBs are the metabolically active and replicative form of *Chlamydia* and divide by binary fission. At the end of every multiplication phase, RBs re-differentiate into EBs to start a new infection cycle (Dautry-Varsat *et al*., 2005; Hybiske and Stephens, 2007). *Sn* has a longer life cycle than other chlamydial species with a replication plateau at day 3 post infection and the release of EBs by host cell-lysis after 5–12 days post infection (Kahane *et al*., 1993; 1999; 2002). Long-term growth is likely connected to inhibition of host cell death induced by *Simkania* infection (Karunakaran *et al*., 2011).

The biogenesis of the chlamydial inclusion and interaction with the host cell have been intensively investigated (for a review, see Fields and Hackstadt, 2002). Once inside the cell, *Chlamydia* resides within a membrane-surrounded host-derived vacuole within the cytoplasm (Hackstadt *et al*., 1997). Shortly after, the vacuole is transported to the microtubule organising centre in a dynein

dependent manner likely through interaction with the dynactin subunit p150(Glued) (Clausen *et al*., 1997; Hackstadt, 2000; Grieshaber *et al*., 2003). Individual inclusions from *C. trachomatis* fuse to form a single large vacuole, whereas many other *Chlamydiales* develop multiple small inclusions (Clausen *et al*., 1997). *Chlamydia* directly modifies the inclusion by secretion of inclusion membrane proteins (Incs) that also extend to the cytosolic face of the inclusion membrane (Rockey *et al*., 1997; Hackstadt *et al*., 1999; Scidmore and Hackstadt, 2001). The action of bacterial proteins in the chlamydial inclusion membrane is assumed to, e.g. prevent endolysosomal fusion, avoid host immune responses and support fusion with sphingomyelin and cholesterol-containing exocytic vesicles from the Golgi apparatus (Scidmore *et al*., 1996b; Ojcius *et al*., 1997; Hackstadt *et al*., 1999; Carabeo *et al*., 2003). It is currently unknown how well conserved basic molecular mechanisms behind these processes are within the order *Chlamydiales*.

Sn forms a continuous membrane system spanning the host cell, and this is clearly distinct from the single vacuolar structure of C*hlamydia* (Mehlitz *et al*., 2014). Interestingly, *Sn* shapes extensive endoplasmic reticulum (ER) contact sites, which are reminiscent of inclusion-ER contact sites also termed pathogen synapses (Derre *et al*., 2011; Dumoux *et al*., 2012; Mehlitz *et al*., 2014). The recent discovery of Inc proteins within other members of the *Chlamydiales*, like *Parachlamydia*, *Waddlia* and *Simkania*, and their low degree of conservation makes it highly likely that the interaction with the host is much more diverse than previously anticipated (Fields and Hackstadt, 2002; Heinz *et al*., 2010; Collingro *et al*., 2011). Only three putative Inc proteins are conserved among *Chlamydiae*, and just a few members can enter and multiply in mammalian cells, indicating a dependency on the host cell type or different molecular mechanisms. The identification and characterisation of Inc or Inc-like proteins in the *Sn* vacuole could reveal the unique molecular interaction with the host ER.

The ER forms a highly branched membrane network arranged in tubes, sheets and cisternae enclosing a fluid-filled interior. Parts of the ER membrane directly associate with the nuclear envelope and extend into the cytosol spanning to the plasma membrane (PM) (English *et al*., 2009). The ER can be divided into smooth and rough ER (SER and RER). RER can easily be identified through lining ribosomes and is associated with multiple cellular functions including protein synthesis, folding or quality control as well as Ca^{2+} homeostasis and regulation of apoptosis (Breckenridge *et al*., 2003; Rizzuto *et al*., 2009; Braakman and Bulleid, 2011). The SER is responsible for vesicle formation, budding and fusion processes, is free of ribosomes and forms a highly complex tubular structure (Shibata *et al*., 2006; Bravo *et al*., 2013). In eukaryotic cells, the ER interacts with the Golgi apparatus through bidirectional vesicle trafficking, co-ordinating cellular protein and lipid transport (Ghaemmaghami *et al*., 2003).

Proteins on donor organelles, e.g. vSNAREs (vesicle soluble N-ethylmaleimide sensitive factor attachment receptor) guide the fusion with the target organelle via interaction with tSNAREs (target SNAREs) (Bonifacino and Glick, 2004). An example of this mechanism is provided by COPI and II vesicles, where COPII vesicles are transported from the ER to the Golgi (anterograde transport) and COPI vesicles are involved in the retrograde backhaul (Brandizzi and Barlowe, 2013). Also non-vesicular mechanisms have been reported for the transfer of proteins and lipids between organelles. Arf1/COPI complexes and the ER to Golgi ceramide transfer protein CERT mediate such non-vesicular transport (Hanada *et al*., 2003; Hanada, 2010; Wilfling *et al*., 2014). This type of transport bridges short distances, e.g. between ER and Golgi membranes, and is required for chlamydial inclusion development (Derre *et al*., 2011; Elwell *et al*., 2011; Dumoux *et al*., 2012). In contrast, data for evolutionary related organisms like *Simkania* are missing. *Simkania* forms numerous ER-vacuole contact sites (Mehlitz *et al*., 2014) and might thereby facilitate uptake of metabolites or lipids required for growth.

Chlamydia requires host-derived lipids like sphingomyelin (SM) and cholesterol for development (Hackstadt *et al*., 1995; Scidmore *et al*., 1996a,b; Carabeo *et al*., 2003). The inclusion membrane thereby constitutes a critical intracellular barrier as these lipids have to be transported into the inclusion to be accessible for the bacteria. As the inclusion membrane is impermeable to small molecules (Heinzen and Hackstadt, 1997), it is thought that *Chlamydia* acquires lipids from vesicles from the secretory pathway that fuse with the inclusion membrane (Carabeo *et al*., 2003; Heuer *et al*., 2009; Derre *et al*., 2011; Elwell *et al*., 2011). This includes the interception of SM-containing Golgi-derived exocytic vesicles destined for the PM or fusion with multivesicular body-derived vesicles (MBV) (Hackstadt *et al*., 1995; Scidmore *et al*., 1996b; Beatty, 2006; 2008; Robertson *et al*., 2009). The latter could also play a role in delivering nutrient into the inclusion that are then taken up by *Chlamydia* via bacterial transporters, permeases and translocases based on active transport processes (Saka *et al*., 2011). Golgi fragmentation induced by *C. trachomatis* has been shown to be important for SM acquisition during the later stages of infection and may be required for subsequent fusion with exocytic vesicles by a mechanism involving Rab6 and Rab11 (Heuer *et al*., 2009; Rejman Lipinski *et al*., 2009).

Here, we established an ER-*Simkania negevensis* containing vacuole (SnCV) isolation protocol to define the

composition of the organelle by label free LC-MS^2. Our data suggest the depletion of components of endosomal trafficking, ER to Golgi as well as exocytic transport in the SnCV. Interestingly, proteins associated with recycling endosomal as well as Golgi to ER transport were enriched in the SnCV, suggesting a role of these pathways in nutrient uptake by *Simkania*. In line with this, interfering with retrograde transport affected *Simkania* replication and SnCV formation. SnCV formation and ceramide acquisition were severely affected by blocking retrograde trafficking underlining the importance of this route for intracellular adaptation of *Simkania*.

Results

Purification of ER-SnCV membranes

Simkania negevensis containing vacuoles are intimately associated with the ER of their host cell (Mehlitz *et al*., 2014). It is unknown how the ER-SnCV interaction is established and whether it affects the composition of the ER. To investigate the effect of infection on the proteome of the ER membranes, the organelle had to be isolated from control and infected cells (Huber *et al*., 2003). We therefore established the isolation of crude ER- and ER-SnCV-membranes from control and *S. negevensis* infected cells (see Fig. 1A and Experimental procedures for more details). Individual isolation steps were analysed by light-microscopy to confirm cell swelling and mechanical rupture (Fig. 1B). Sequential centrifugation steps led to the fractionation into pre-nuclear (PNF), pre-mitochondrial (PMF) and crude microsomal ER-fraction (CMF) (Fig. 1A). The quality of the ER-SnCV membrane purification was controlled by immunoblotting by detecting marker proteins for cytoskeleton (ß-Actin), mitochondria (Sam50) and nuclei (Lamin B1) (Fig. 1C). Calnexin an ER membrane protein was detected within PMF and CMF fractions indicating the strong association of the ER with organelles like mitochondria (Fig. 1C). A subset of soluble ER proteins like PDI and ERp72 were found in the PMF and only to a low extend in the CMF, which could be due to association with other organelles (Fig. 1C). KDEL (Lys-Asp-Glu-Leu) ER retention signal containing proteins were selectively enriched in the CMF (Fig. 1C). Bacteria were strongly depleted from the CMF as was monitored by detecting the bacterial heat shock protein GroEL (Fig. 1C). Residual GroEL was most likely derived from broken bacteria, as intact bacteria were hardly detectable in the CMF by transmission electron microscopy (TEM) (Fig. 1D). Interestingly, we observed only a fraction of total bacterial proteins within the CMF fraction likely representing bacterial proteins localised to the SnCV membrane (Fig. 1C). These results show the isolation of crude ER-SnCV membranes from *Simkania* infected cells as well as the modulation of the ER composition through *Simkania* infection.

Proteome analysis of crude ER-SnCV membranes (CMF)

We then analysed the crude ER-SnCV membrane fraction (CMF) of three biological replicates by LC-MS^2 to identify *Simkania* infection-mediated changes of ER composition and identified 1178 human and 302 *Simkania* proteins in the infected samples (Fig. 2A and Supplementary Tables S1 and S3). One hundred twenty-three out of 302 (41%) identified bacterial proteins were hypothetical proteins with no known function or homology upon database searches respectively (Supplementary Table S3). Inc proteins are highly species-specific proteins and can be predicted applying the following criteria: (i) hypothetical protein, (ii) no Sec-signal and (iii) bi-lobed hydrophobicity profile (Collingro *et al*., 2011). Twenty-three out of 123 hypothetical proteins (19%) fulfilled these criteria supporting the co-purification of ER and SnCV (Supplementary Table S3). We next grouped the remaining 179 proteins according to known function or subcellular localisation: 16% of the proteins were ribosomal components, 11% were localised in the bacterial cytoplasm and 9% were membrane proteins or belonged to RNA-polymerase, proton transport, cell surface, helicase or acetyl-CoA carboxylase complex (Supplementary Table S3). More interestingly, 20% of the proteins were associated with type III or Sec-system according to Uniprot and Effectors databases (Supplementary Table S3). We did not detect any components of the *Simkania* type IV secretion system. Comparison of identified proteins with published pan-genome data (Collingro *et al*., 2011) showed that 11 out of the 302 identified proteins are *Simkania* specific factors (11/11 hypothetical, 4/11 located on the plasmid pSN), 16/302 proteins showed homologs in *Chlamydia* and 12/302 proteins are virulence associated, e.g. LPS synthesis proteins or macrophage infectivity potentiator (Supplementary Tables S4 and S5).

The potential subcellular localisation of the identified human proteins was predicted by database searches using WEB-based Gene SeT AnaLysis (WEB-Gestalt) toolkit (Wang *et al*., 2013) (Fig. 2B). Most of these proteins were predicted by GO annotation as part of macromolecular complexes, membrane enclosed lumen and membrane of the nucleus, cytosol, mitochondria, cytoskeleton, endomembrane system and ER (Fig. 2B). We then performed an enrichment analysis using WEB-Gestalt and GO analysis against the human genome as a reference set and standard settings with the exception of top10 significance level and minimum of 10 genes per category. Enrichment analysis confirmed isolation of ER-targeted proteins in comparison with the total genome

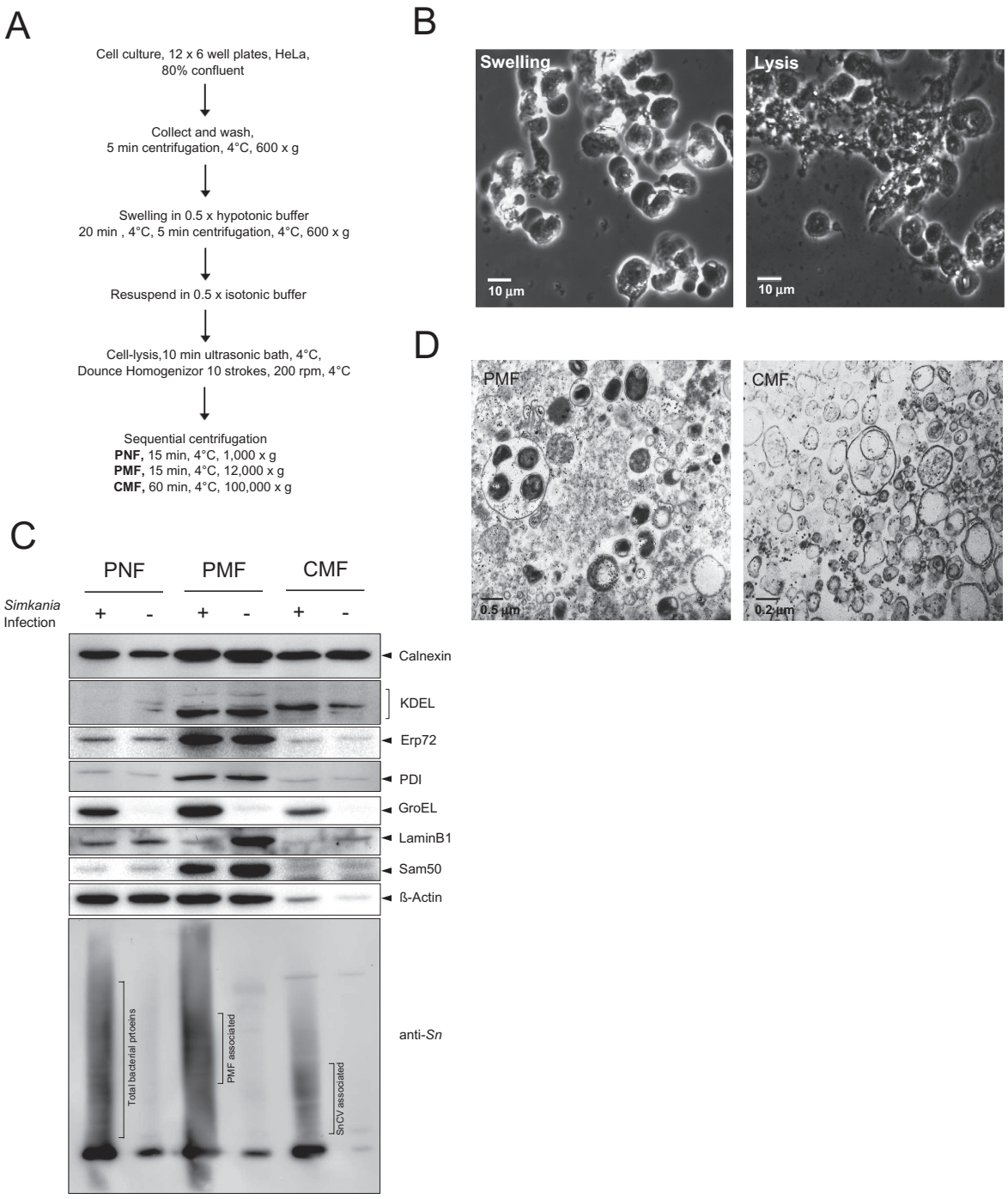

Fig. 1. Purification of *Simkania*-containing vacuole (SnCV) and ER membranes.
A. Flowchart showing purification of ER-SnCV-membranes. ER-SnCV-membranes were purified from infected HeLa cells by successive swelling and lysis steps followed by three sequential centrifugation steps.
B. Phase contrast microscopy of swelling and lysis steps described in A. Cells were equally swollen and visibly broken by mechanical lyses.
C. Immunoblot analysis of purified membrane fractions. Composition of the purified ER-SnCV-membranes is shown by various marker proteins. Purification led to isolation of mainly ER membrane associated (Calnexin and KDEL) and bacterial proteins (anti-*Sn*) in the final fraction (CMF). Soluble ER proteins (Erp72 and PDI) and markers for other cell compartments like mitochondria (Sam50), nuclei (Lamin B1) and cytoskeleton (ß-Actin) are excluded from the CMF.
D. Transmission electron microscopy of infected PMF (left) and CMF (right) fractions. While the PMF still contained both intact *Simkania* and mitochondria, the CMF is devoid of intact bacteria, indicating that purified bacterial proteins might be membrane-associated secreted proteins.
Min = minutes, PNF = pre-nuclear fraction, PMF = pre-mitochondrial fraction, CMF = crude microsomal fraction.

validating the crude ER-SnCV fraction (CMF) used for the analysis (Supplementary Fig. S1). Most of the other significantly enriched categories were found to be involved in, e.g., RNA processing and translation (Supplementary Fig. S1).

The proteome data were further classified by function like, e.g., protein-, nucleic acid-, ion and metabolic binding and various enzymatic functions (Fig. 2C). Categorisation by cellular process indicated that the identified proteins are involved mainly in metabolic processes but also cellular component organisation and responses to various stimuli (Fig. 2D). We next tested for differential expression in spectral counts between infected and non-infected samples after adjusting for sample effects using the edgeR statistical package. A large number of proteins with a nominal P-value < 0.05 could be identified (Supplementary Table S2). Comparing the expression of infection-associated genes across all three samples indicated that infection in sample 3 did not work (Supplementary Fig. S2). We focused our further analysis on samples 1 and 2, which show similar infection-induced regulatory patterns (Fig. 3A). Six proteins (2'-5'-oligoadenylate synthase 3, Heterogeneous nuclear ribonucleoproteins A2/B1, Voltage-dependent anion-selective channel protein 1, ATP synthase subunit beta, Heterogeneous nuclear ribonucleoprotein A0 and ATP synthase subunit alpha) were differentially regulated after adjusting P-values for multiple testing (Supplementary Table S2). To allow for explorative network analysis, we lowered the threshold of adjusted P-value to < 0.2 now taking into account 51 differentially expressed genes (Supplementary Tables S2 and S6). Ingenuity analysis categorised these proteins into 21 significant categories, with the top canonical pathways being involved in mitochondrial dysfunction, oxidative phosphorylation, tRNA charging, telomere extension by telomerase and acetyl-CoA biosynthesis III (Fig. 3B). Network connectivity analysis of these 51 proteins resulted in three major networks (Fig. 3C–E). We observed a large number of mitochondrial proteins (F1 ATPase, ATP5A1, ATP5B, ATP5O, ATP5F1, ATP synthase, VDAC1, TOMM40, UOCRC2) depleted from the ER/SnCV fraction (Fig. 3C). Similarly, anterograde transport components (Rab1A, Rab14, Sec22B) appeared to be depleted in infected cells (Fig. 3C). Cytoskeletal components and regulators (ARHGEF2, MSN) especially cytokeratins appear to be de-regulated (enriched: KRT6A, Cytokeratin, KRT5, depleted: KRT8, KRT18) while myosins are depleted (MYH10, Myosin 2) in ER/SnCV from infected cells (Fig. 3C–E). Taken together, these results provide an overview of the proteins regulated in the ER and associated organelles of *Simkania*-infected cells.

Some differentially regulated proteins obtained by LC-MS^2 and statistical testing were validated by immunoblot (Fig. 3F and G). Interestingly, we observed an enrichment of CCT2 (cytosolic T-complex 1 subunit beta, TCP-1-B), which forms a complex with CCT1 (cytosolic T-complex 1 subunit alpha, TCP-1-A) in ER/SnCV fractions (Fig. 3G). ARHGEF2 (Rho guanine nucleotide exchange factor 2, GEF H1) was also found to be enriched in purified membranes from infected cells (Fig. 3G) confirming our mass spectrometry approach (Fig. 3A, C–E, Supplementary Tables S1 and S2). Enrichment of ARHGEF2 and CCT2 at day 3 post infection was not apparent in whole cell lysates of time course experiments, validating that enrichment/depletion analysis is not merely due to overall expressional changes within the cell. In contrast, we also tested for vesicle-associated membrane protein 2 (VAMP2), voltage-dependent anion channel 1 (VDAC1) and translocase of outer mitochondrial membrane 40 (TOMM40) and could confirm depletion on day 3 post-infection both on ER/SnCV as well as whole cell level (Fig. 3F and G). These results demonstrate that identification and quantification of these proteins by mass spectrometry and statistical prediction of protein regulation for day 3 post infection correlated with protein levels in ER/SnCV membranes detected by immunoblotting.

Endosomal trafficking is required for progeny formation

Chlamydia has developed mechanisms to avoid lysosomal degradation and acquire lipids via interception of Golgi-derived sphingomyelin-rich vesicles (Hackstadt *et al.*, 1995; Scidmore *et al.*, 2003). As acquiring lipids by modulation of cellular trafficking is absolutely essential for *Chlamydia* and proteins associated with anterograde transport appear to be depleted from the ER/SnCV fraction (Fig. 3C), we systematically searched our proteomics data for factors involved in vesicular trafficking. We detected several additional major regulators of endosomal trafficking (Supplementary Tables S1 and S7). STRING-based network analysis (von Mering *et al.*, 2003) of these hits showed that endosomal and exocytic transport as well as COPII-dependent and -independent ER to Golgi transport were depleted from the ER/SnCV fraction upon infection with *Simkania* (Fig. 4A and corresponding values in Supplementary Table S7). In contrast, proteins of the endosomal recycling pathway were mainly unchanged, whereas COPI transport was partially enriched (Fig. 4A). Clathrin-dependent Golgi to ER transport proteins were enriched in ER/SnCV (Fig. 4A).

This pattern of regulation indicated that *Simkania* might require retrograde transport via clathrin- and Golgi-associated vesicles for nutrient/metabolite acquisition and growth. To test this assumption, we performed infectivity assays in cells, which were treated with inhibitors of retrograde trafficking (Retro-1, Retro-2 and VP-184). Retro-1 and Retro-2 have been selected on their activity to interfere with retrograde transport of ricin toxin and Shiga

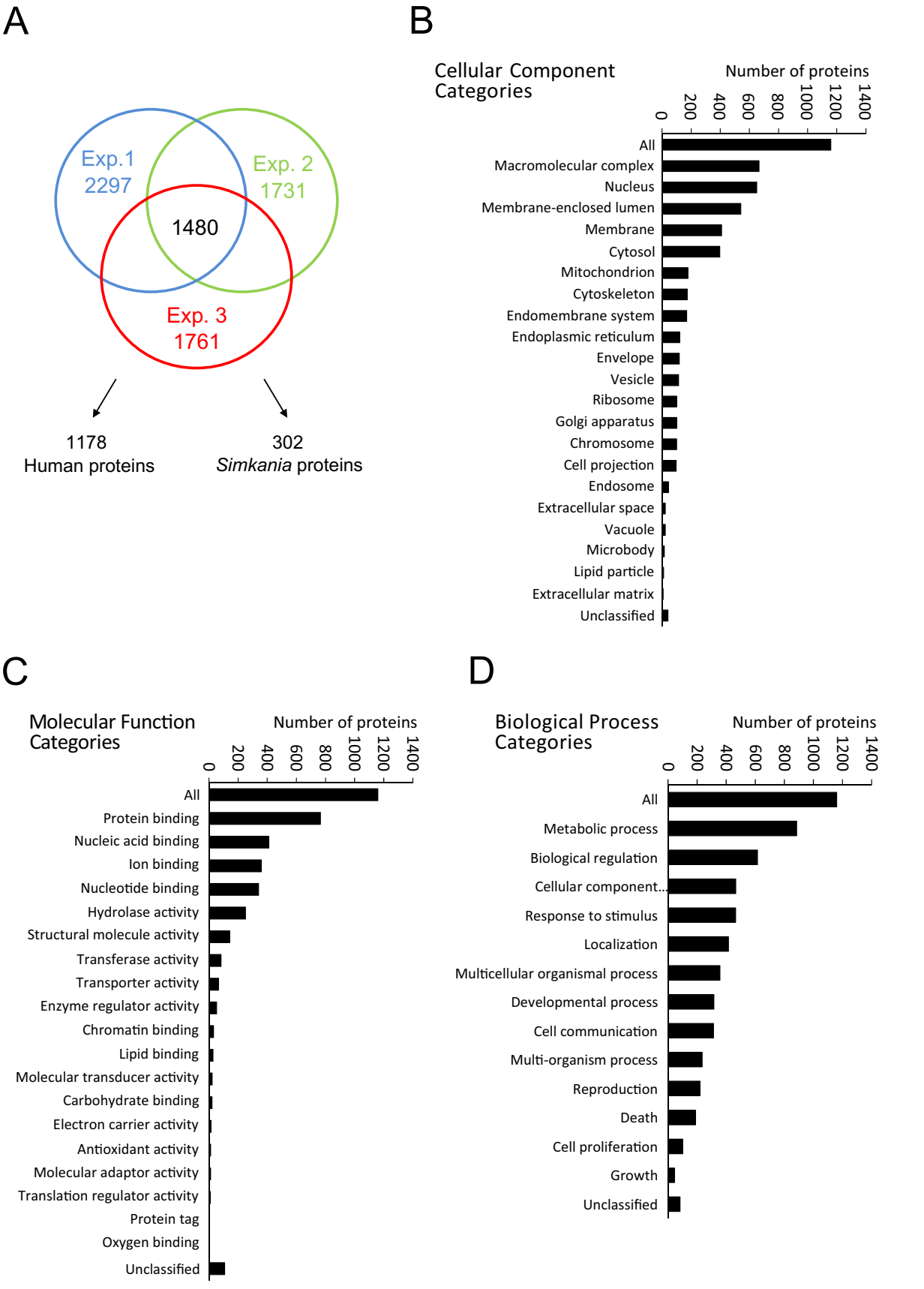
A
Exp.1
2297
Exp. 2
1731
1480
Exp. 3
1761
1178
Human proteins
302
Simkania proteins
B
Cellular Component
Categories
Number of proteins
0
200
400
600
800
1000
1200
1400
All
Macromolecular complex
Nucleus
Membrane-enclosed lumen
Membrane
Cytosol
Mitochondrion
Cytoskeleton
Endomembrane system
Endoplasmic reticulum
Envelope
Vesicle
Ribosome
Golgi apparatus
Chromosome
Cell projection
Endosome
Extracellular space
Vacuole
Microbody
Lipid particle
Extracellular matrix
Unclassified
C
Molecular Function
Categories
Number of proteins
0
200
400
600
800
1000
1200
1400
All
Protein binding
Nucleic acid binding
Ion binding
Nucleotide binding
Hydrolase activity
Structural molecule activity
Transferase activity
Transporter activity
Enzyme regulator activity
Chromatin binding
Lipid binding
Molecular transducer activity
Carbohydrate binding
Electron carrier activity
Antioxidant activity
Molecular adaptor activity
Translation regulator activity
Protein tag
Oxygen binding
Unclassified
D
Biological Process
Categories
Number of proteins
0
200
400
600
800
1000
1200
1400
All
Metabolic process
Biological regulation
Cellular component...
Response to stimulus
Localization
Multicellular organismal process
Developmental process
Cell communication
Multi-organism process
Reproduction
Death
Cell proliferation
Growth
Unclassified

Fig. 2. Analysis of the proteome data.
A. Venn diagram indicating the number of proteins identified by LC-MS^2. The 1,480 proteins were identified, 1,178 of human and 302 of *Simkania* origin ($n = 3$).
B. Cellular component histogram displays the distribution of the identified human proteins across sub-cellular localisation. Categorisation is based on GO-annotations allowing multiple localisations. Most proteins are associated with macromolecular complex, membrane enclosed lumen and membrane. Top sub-cellular localisations were nucleus, cytosol, mitochondrion, endomembrane system and endoplasmic reticulum.
C. Categorisation by molecular function using GO-annotation, multiple terms per protein allowed. Most proteins were associated with metabolite binding and exerted enzymatic activities.
D. Analysis via biological process histogram using GO-annotations and allowing multiple term per proteins shows that most of the proteins identified are associated with metabolic functions of the host cell.

toxins (Stechmann *et al*., 2010; Noel *et al*., 2013). VP-184 is a Retro-1 analogue giving increased protection against Shiga toxins (J.B. and V.P., unpublished data). Primary infection measured by inclusion size was slightly reduced by the inhibition of endosome to Golgi transport using Retro-1 and -2 (Fig. 4B and C). VP-184 strongly reduced primary infection and inclusion size at higher concentrations (Fig. 4B and C). Interestingly, all inhibitors strongly interfered with progeny formation (Fig. 4B, D and E). In this assay, bacteria are first grown in cells treated with inhibitors, and the infectious particles from this primary infection are applied to fresh cells in the absence of inhibitor to measure the bacterial load (GroEL immunoblot) and inclusion formation (immunofluorescence microscopy). Thus, all three Retro compounds affect *Simkania* infection and SnCV formation during primary infection and progeny formation.

Next, we performed RNA interference experiments to specifically address the role of several target proteins. We concentrated on syntaxin 5 (STX5) (a potential host target of Retro compounds), coatomer protein complex subunit 2 (COPB2), adaptor-related protein complex 2 subunit beta1 (AP2B1) and ARHGEF2 (Figs 3C and 4A). Knockdown efficiency was tested by qRT-PCR and found to be 86% (COPB2), 74% (ARHGEF2), 96% (STX5) and 98% (AP2B1) (data not shown). Immunoblot analysis of infected transfected cells showed no changes in primary infection for ARHGEF2, whereas knockdown of COPB2 (37%), STX5 or AP2B1 (26% or 13%) reduced primary infection (Fig. 6F). Interestingly, silencing COPB2 and AP2B1 expression reduced *Simkania* progeny formation (27–34%) (Fig. 6F). Taken together, these data confirm the important role of retrograde trafficking for infection with *Simkania*.

Inhibitors of retrograde trafficking cause phenotypic variations in SnCV formation

Bacterial AB$_5$-toxins, like Cholera- and Shiga toxins, are transported along the retrograde route from the PM to the trans-Golgi network (TGN) to reach the ER (Sandvig and van Deurs, 2002). Retro-1 and -2 specifically block the early endosome-to-Golgi transport of these toxins without affecting essential endogenous cargo proteins, protein biosynthesis or morphology of the ER (Stechmann *et al*., 2010; Ming *et al*., 2013; Noel *et al*., 2013). As all tested inhibitors of retrograde transport have had an effect on primary and progeny infection for *Simkania* (Fig. 4B–E), we inspected the subcellular structure of infected cells by TEM (Fig. 5). A strong inhibition of *Simkania* replication was observed at a concentration of 75 μM for Retro-1, -2 and 25 μM for VP-184 (Fig. 4B–E). SnCVs formed normally in DMSO-treated control cells (Fig. 5A). The SnCV was smaller in Retro-1-treated cells, and less sub-vacuoles were visible (Fig. 5B). Retro-2 affected the SnCV morphology as sub-vacuolar membranes were highly enlarged and contained excessive membrane material, probably as a consequence of defective membrane fusion and vacuole formation (Fig. 5C). Parts of the enlarged sub-vacuoles contained just few bacteria located at the inclusion boundary, which may indicate defective *Simkania* replication. Additionally, sub-vacuoles were surrounded by multiple membranes at several areas indicative of a role of Retro-2 inhibited pathways in SnCV formation and membrane fusion defect. VP-184 seemed to have an effect on cell growth and development because infected cells appear smaller than control cells (Fig. 5D). In line with this, SnCV size and morphology was also affected in about half of the cells (Fig. 4C). Surprisingly, sub-vacuoles contained small transparent vesicles of unknown origin and mitochondria were associated with vesicular structures similar to lipid droplets. Again cellular effects caused by VP-184 strongly influence SnCV formation and *Simkania* replication. The discovery of vesicular structures inside the SnCV and at the mitochondria indicated a possible shift in lipid metabolism. In summary, all three Retro compounds have unique effects on the SnCV morphology suggesting that retrograde transport is essential for normal development of *Simkania*.

Inhibitors of retrograde trafficking affect ceramide transport to the Golgi and the SnCV

Chlamydia acquire lipids for inclusion formation and intracellular replication from secretory pathways (van Ooij *et al*., 2000; Carabeo *et al*., 2003; Heuer *et al*., 2009; Derre *et al*., 2011; Elwell *et al*., 2011), e.g. by interception of SM-containing Golgi-derived exocytic vesicles

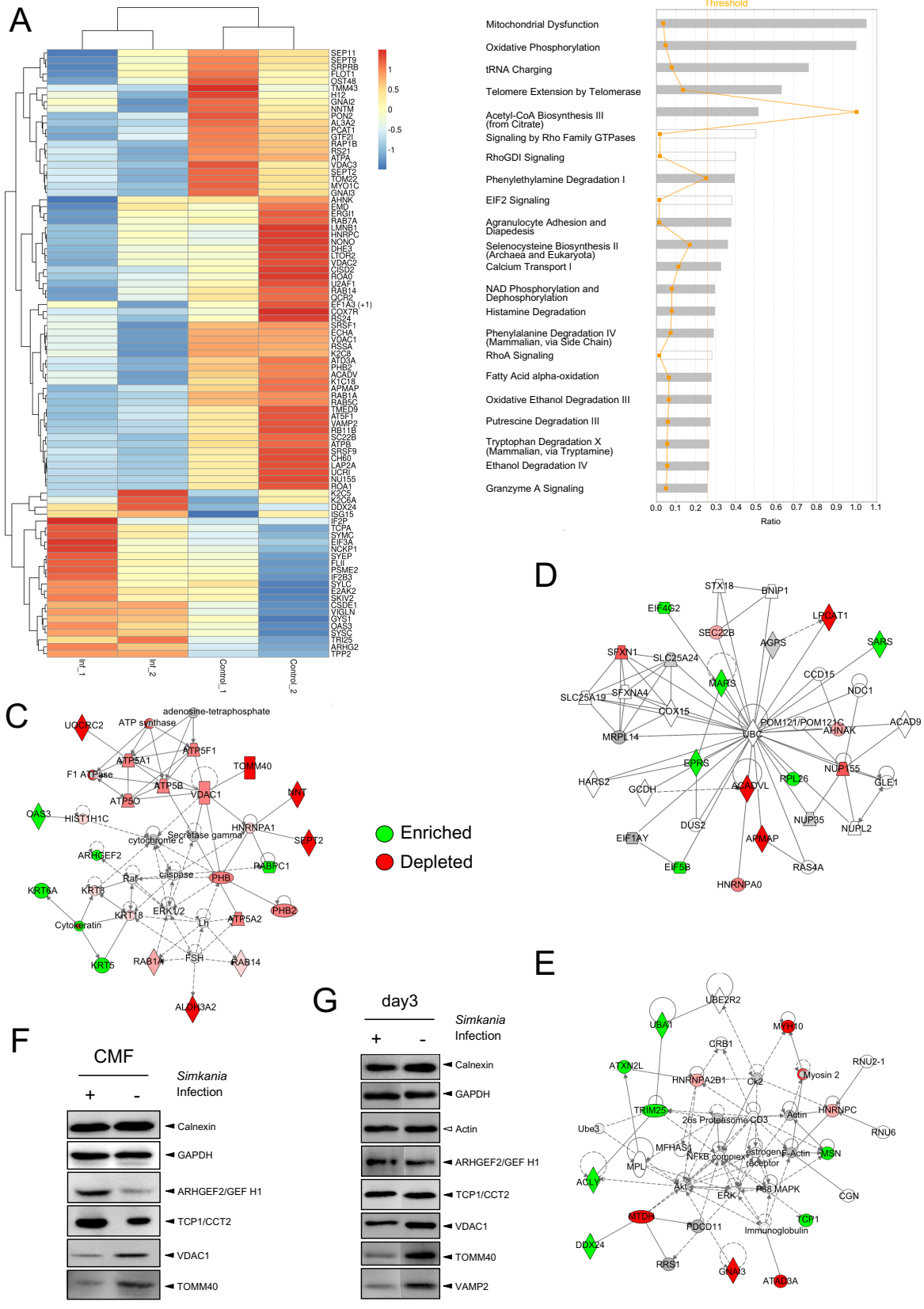
A
Inf_1
Inf_2
Control_1
Control_2
B
z-score = 0
no activity pattern available
Ratio
-log (p-value)
Threshold
Mitochondrial Dysfunction
Oxidative Phosphorylation
tRNA Charging
Telomere Extension by Telomerase
Acetyl-CoA Biosynthesis III (from Citrate)
Signaling by Rho Family GTPases
RhoGDI Signaling
Phenylethylamine Degradation I
EIF2 Signaling
Agranulocyte Adhesion and Diapedesis
Selenocysteine Biosynthesis II (Archaea and Eukaryota)
Calcium Transport I
NAD Phosphorylation and Dephosphorylation
Histamine Degradation
Phenylalanine Degradation IV (Mammalian, via Side Chain)
RhoA Signaling
Fatty Acid alpha-oxidation
Oxidative Ethanol Degradation III
Putrescine Degradation III
Tryptophan Degradation X (Mammalian, via Tryptamine)
Ethanol Degradation IV
Granzyme A Signaling
Ratio
C
adenosine-triphosphate
ATP synthase
ATP5F1
ATP5A1
F1 ATPase
TOMM40
ATP5B
VDAC1
ATP5O
NAT
HIST1H1C
HNRNPA1
Secretase gamma
cytochrome c
SEPT2
ARHGEF2
PABPC1
caspase
PHB
Raf
KRT8
KRT18
ERK1/2
PHB2
Cytokeratin
ATP5A2
KRT5
RAB1A
PSH
RAB14
ALDH3A2
Enriched
Depleted
D
STX18
BNIP1
EIF4G2
LPCAT1
SEC22B
AGPS
SARS
SFXN1
SLC25A24
CCD15
MARS
SLC25A19
SFXNA4
NDC1
COX15
POM121/POM121C
ACAD9
AHNAK
MRPL14
UBC
EPRS
NUP155
HARS2
GCDH
ACADVL
RPL26
GLE1
DUS2
NUP35
NUPL2
EIF1AY
ARMAP
EIF5B
RAS4A
HNRNPA0
E
UBE2R2
UBA1
MYH10
CRB1
RNU2-1
ATXN2L
HNRNPA2B1
CK2
Myosin 2
TRIM25
26s Proteasome-CD3
Actin
HNRNPC
Ube3
RNU6
MFHAS1
NFkB complex
Estrogen Receptor
F-Actin
MSN
MPL
AOC1
Akt
ERK
P38 MAPK
CGN
MTDH
PDCD11
TCP1
Immunoglobulin
DDX24
RRS1
GNAI3
ATAD3A
F
CMF
Simkania Infection
+
-
Calnexin
GAPDH
ARHGEF2/GEF H1
TCP1/CCT2
VDAC1
TOMM40
G
day3
Simkania Infection
+
-
Calnexin
GAPDH
Actin
ARHGEF2/GEF H1
TCP1/CCT2
VDAC1
TOMM40
VAMP2

Fig. 3. Network analysis of proteome data.
A. Heatmap of sample adjusted spectral counts (samples 1 and 2), of edgeR differentially expressed proteins only (raw *P*-value < 0.05 to 0.2).
B. Pathway enrichment of 51 proteins with adjusted *P*-values ≤ 0.2 analysed with the Ingenuity software (see Supplementary Table S2). Bars show the –log (*P*-value) for the enrichment of proteins of a given group within the list of selected proteins using a right-tailed Fisher's exact test. Orange squares show the ratio of proteins detected (within the selected list) among all proteins associated with that group.
C–E. Proteins were clustered into networks of protein–protein interaction based on Ingenuity analysis. Network clustering show e.g. (C) downregulation of mitochondrial proteins and anterograde transport, de-regulation of cytoskeletal components, (D) upregulation of tRNA charging and (E) various metabolic functions. The intensity of green and red molecule colours indicates the degree of depletion or enrichment respectively. Symbols reflect protein class e.g. enzyme and connections depict the way proteins interact (see Supplementary Fig. S5 for additional information).
F. Immunoblot analyses of crude purified ER-SnCV (CMF) membrane fractions. Calnexin and glycerinaldehyde-3-phosphate dehydrogenase (GAPDH) were unchanged in ER-SnCV membranes after infection; T-complex 1 related (TCP1/CCT2) and Rho guanine nucleotide exchange factor 2 (ARHGEF2/GEF H1) were enriched; voltage dependent anion channel 1 (VDAC1) and translocase of outer mitochondria membrane 40 (TOMM40) were depleted.
G. Immunoblot analyses of whole cell lysates from 3 day time-course experiments of infected and control cells. Calnexin and GAPDH are unchanged in whole cell lysate at 3 days post infection. ARHGEF2/GEF H1 is weakly enriched, TCP1/CCT2 is unchanged, whereas VDAC1, TOMM40 and VAMP2 (vesicle-associated membrane protein 2) are depleted during infection. Actin was used as loading control.

(Hackstadt *et al*., 1995; Scidmore *et al*., 1996b; Beatty, 2006; 2008; Robertson *et al*., 2009). To test if inhibitors of retrograde transport directly affect cellular transport processes to the SnCV, we analysed lipid transport using the fluorescent ceramide derivative C_6-NBD-ceramide in live cell imaging experiments (Fig. 6A–F, Supplementary Figs S3 and S4). This fluorescent ceramide provides a vital stain for the Golgi apparatus (Lipsky and Pagano, 1985b; Pagano *et al*., 1989; Rosenwald and Pagano, 1993) and is also transported to *Chlamydia* inclusions (Hackstadt *et al*., 1995). NBD-labelled-glucosylceramide and -sphingomyelin are transported from the PM retrograde to the Golgi complex across early and recycling endosomes (Babia *et al*., 2001). C_6-NBD-ceramide transport to Golgi (mRFP-labelled) and SnCV was monitored over a time period of 30 min at 1 frame/30 s (Fig. 6A–C) in the absence or presence of inhibitors of retrograde transport or the previously described Golgi disrupting agent Brefeldin A (BFA) (Hackstadt *et al*., 1995; Scidmore *et al*., 1996a; Babia *et al*., 2001) (Fig. 6D–F, Supplementary Figs S3 and 4). As expected, the C_6-NBD-ceramide transfer to mRFP-fluorescent Golgi followed a kinetic similar to carrier-mediated transport. Signal intensity at the Golgi was lower during infection but followed a similar kinetic (Fig. 6A). Fluorescent ceramide that was not taken up by the Golgi and/or the SnCV was detected in the cell cytosol (Fig. 6B and C). Analyses of untreated ER-KDEL fluorescent cells showed that C_6-NBD-ceramide transport ends at the Golgi apparatus and does not reach the ER (Supplementary Fig. S3A). C_6-NBD-ceramide transport was faster and signal intensity increased at the Golgi in VP-184-treated non-infected cells compared with control (Fig. 6D and Supplementary Fig. S3E). In contrast, *Simkania*-infected cells showed a strongly reduced C_6-NBD-ceramide transport to the Golgi in the presence of VP-184 (Fig. 6E, Supplementary Fig. S4B). In accordance with this observation, VP-184 also strongly reduced the C_6-NBD-ceramide signal at the SnCV (Fig. 6F, Supplementary Fig. S4B). C_6-NBD-ceramide slightly accumulated in the Golgi in Retro-2-treated cells and infection strongly increased this effect (Fig. 6D and E, Supplementary Figs S3D and S4D). Thus, Retro-2 seemed to optimise retrograde lipid-trafficking to the Golgi *per se* but especially during infection. This was also observed at the level of C_6-NBD-ceramide SnCV transport, which was increased in Retro-2-treated cells (Fig. 6F, Supplementary Fig. S4D). Retro-1 had the similar although milder effect as Retro-2 (Fig. 6D–F, Supplementary Figs 3C and 4C). BFA causes disassembly of the Golgi apparatus and thereby is expected to block C_6-NBD-ceramide uptake by the Golgi. We observed Golgi fragmentation 30 min after BFA treatment that was followed by reduced fluorescent lipid uptake and Golgi transport in both non-infected and infected cells (Fig. 6D and E, Supplementary Figs 3B and 4A). Interestingly, the SnCV showed reduced but not completely abolished C_6-NBD-ceramide levels in the presence of BFA (Fig. 6F). This result indicates possibly a secondary lipid-transport route to the *Simkania* inclusion. Thus, the Retro compounds affect C_6-NBD-ceramide transport to the Golgi and to the SnCV, which may explain their effect on SnCV morphology and bacterial development.

Discussion

Proteomic analysis of isolated pathogen containing vacuoles has been successfully applied to many different bacteria to characterise these unique cellular compartments (Herweg *et al*., 2015). Proteome analysis of the *Chlamydia*-containing vacuole revealed the recruitment of host cell PM receptors and retromer complexes (Aeberhard *et al*., 2015; Mirrashidi *et al*., 2015; Subbarayal *et al*., 2015). Here, we applied a proteomics approach to investigate the composition of the SnCV and the host ER with the aim to identify changes in protein composition that could give us hints on the intracellular accommodation of *Simkania*. A crucial step towards this aim was the crude purification of the SnCV together with ER membranes, which was probably possible due to a close association of

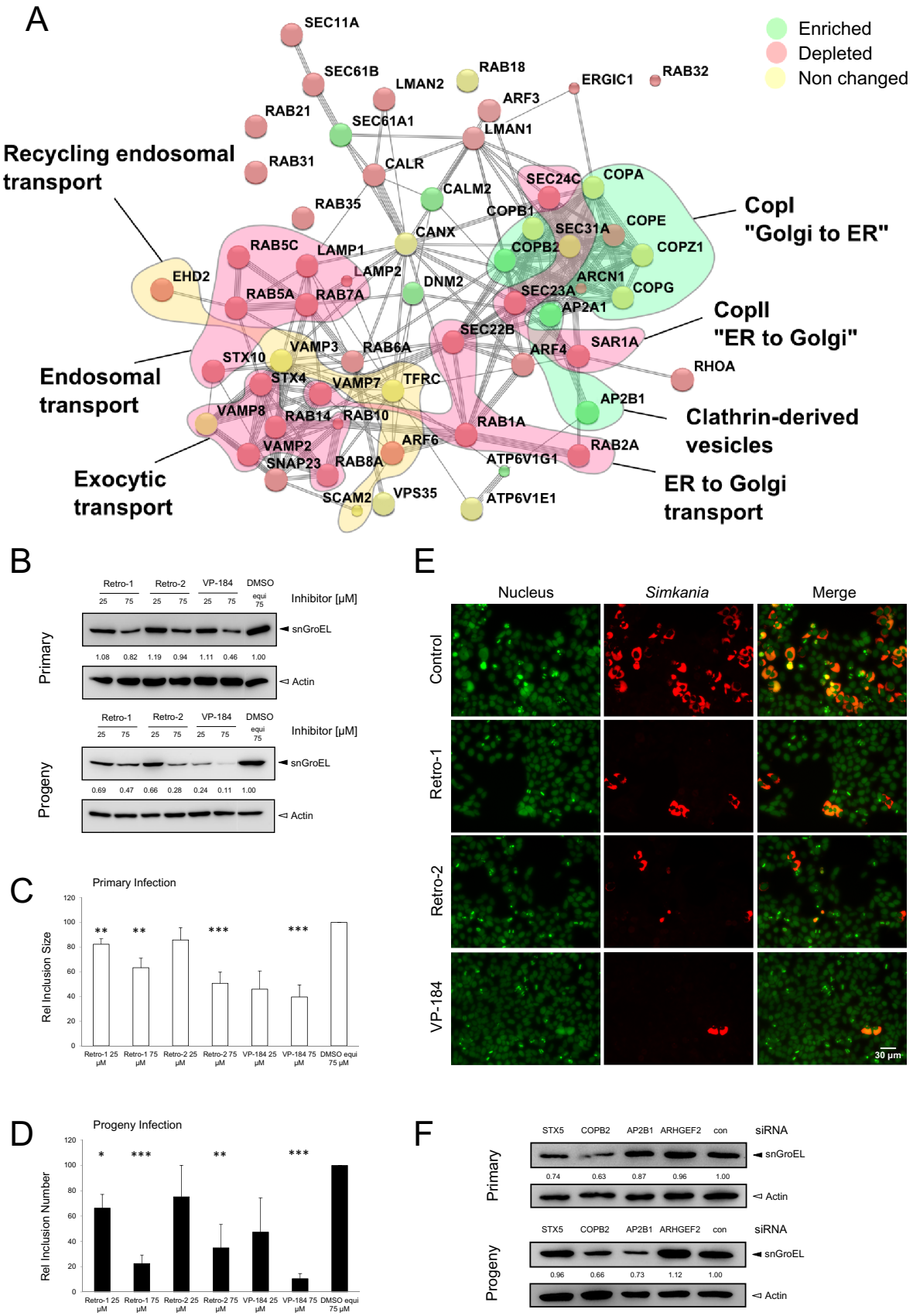
A
Enriched
Depleted
Non changed
SEC11A
SEC61B
LMAN2
RAB18
ERGIC1
RAB32
ARF3
RAB21
SEC61A1
LMAN1
Recycling endosomal transport
RAB31
CALR
SEC24C
COPA
CALM2
RAB35
COPB1
SEC31A
COPE
CopI "Golgi to ER"
CANX
RAB5C
LAMP1
COPB2
COPZ1
LAMP2
EHD2
DNM2
ARCN1
RAB5A
RAB7A
SEC23A
COPG
AP2A1
CopII "ER to Golgi"
SEC22B
SAR1A
VAMP3
RAB6A
ARF4
STX10
RHOA
Endosomal transport
STX4
VAMP7
TFRC
AP2B1
VAMP8
RAB14
RAB10
RAB1A
Clathrin-derived vesicles
ARF6
VAMP2
RAB2A
SNAP23
RAB8A
ATP6V1G1
Exocytic transport
ER to Golgi transport
SCAM2
VPS35
ATP6V1E1
B
Retro-1
Retro-2
VP-184
DMSO equi
Inhibitor [μM]
25
75
Primary
snGroEL
1.08 0.82 1.19 0.94 1.11 0.46 1.00
Actin
Progeny
0.69 0.47 0.66 0.28 0.24 0.11 1.00
C
Primary Infection
Rel Inclusion Size
Retro-1 25 μM
Retro-1 75 μM
Retro-2 25 μM
Retro-2 75 μM
VP-184 25 μM
VP-184 75 μM
DMSO equi 75 μM
D
Progeny Infection
Rel Inclusion Number
E
Nucleus
Simkania
Merge
Control
Retro-1
Retro-2
VP-184
30 μm
F
STX5
COPB2
AP2B1
ARHGEF2
con
siRNA
Primary
0.74 0.63 0.87 0.96 1.00
Progeny
0.96 0.66 0.73 1.12 1.00

Fig. 4. Regulation of endosomal and retrograde trafficking during *Simkania* infection. Filtering of the proteomic data showed that 57 human proteins are involved in cellular transport processes e.g. endosomal and exocytic trafficking (see Supplementary Table S7).
A. STRING-based protein network analysis highlights sub-networks of similar regulation representative of different cellular transport routes. Enriched (green) (Kahane *et al*.) and depleted (red) (Bravo *et al*.) proteins (regulation > ± 0.20 logFC) are clustered in several sub-networks involved in COPII-/ER to Golgi, exocytic, recycling endosomal, endosomal, clathrin and COPI (Golgi to ER) transport. Unchanged (yellow) proteins (regulation < –0.20 logFC) mostly form loosely network nodes. Several Golgi to ER and clathrin-derived vesicle proteins were enriched or unchanged, whereas ER to Golgi, endosomal and exocytic proteins were depleted.
B. HeLa cells were infected with *Simkania* at moi 0.5 for 3 days in the presence of inhibitors of retrograde trafficking (Retro-1, Retro-2 and VP-184). Immunoblots show bacterial growth via *Simkania* GroEL (snGroEL) levels in primary as well as progeny infection. Primary infection decreased in the presence of Retro-1 and -2 inhibitors of retrograde trafficking. The negative effect on bacterial replication mediated through Retro-1 and -2 became more pronounced in progeny formation. VP-184 showed a more pronounced effect during primary infection and strongly prevented formation of infective progeny. ß-Actin was used as protein loading control.
C–D. Bar diagram showing the analysis of infectivity assays from cells treated as described in B. $P \leq 0.05$ = *, $P \leq 0.01$ = **, $P \leq 0.001$ = ***, $n = 4$. (C) Relative inclusion size of *Simkania*-containing vacuoles (SnCVs) was detected by using ImageJ. The average size of SnCVs decreased upon Retro compound treatment. (D) Analysis of inclusion number from progeny infection. As observed in B. reduction in inclusion number became more pronounced in progeny infection.
E. Immunofluorescence images of HeLa progeny cells after 3 days incubation. Nuclei were stained for DAPI (green) (Kahane *et al*.) and SnCVs were stained for GroEL (red) (Bravo *et al*.). Inhibitor-treatment reduced *Simkania* progeny formation. (B–E) Images are representative of $n = 3$ independent experiments.
F. HeLa cells were RNAi treated (STX5, ARHGEF2, COPB2, AP2B1 or AllStars negative control) and infected with *Simkania* at moi 0.5 for 3 days. Immunoblots show bacterial growth via snGroEL levels in primary as well as progeny infection. Primary infection was decreased in COPB2 and slightly decreased in STX5 or AP2B1 knockdown. Interestingly, COPB2 as well as AP2B1 decreased progeny formation. ß-Actin was used as loading control, $n = 3$.

these membranes and ER contact sites. Although direct information on trafficking pathways cannot be deduced from these proteomics data, the composition of the compartment can be estimated. We could use these semi-quantitative data and protein interaction predictions to identify complex networks of interacting proteins including transport processes with infection-dependent enrichment or depletion.

Intracellular pathogens frequently escape from the phagolysosomal route to prevent lysosomal degradation. Although initially believed to be exceptions, pathogen-containing compartments with ER or Golgi features (Desjardins, 2003) have been meanwhile demonstrated for the important pathogens *Brucella* (Anderson and Cheville, 1986; Pizarro-Cerda *et al*., 1998), *Legionella* (Horwitz, 1983; Swanson and Isberg, 1995; Tilney *et al*., 2001) and *Chlamydia* that replicate in vacuoles receiving lipids from the TGN (Heinzen *et al*., 1996). *Legionella* and *Brucella* interfere with the biogenesis of the early phagolysosome modulating their vacuolar composition to mature into in ER-derived compartments (Desjardins, 2003). Like many other bacteria, all *Chlamydiae* develop and multiply within a unique vacuole, which is not acidified (Friis, 1972; Lawn *et al*., 1973; Wyrick and Brownridge, 1978; Heinzen *et al*., 1996; Al-Younes *et al*., 1999; Rockey *et al*., 2002). However, also *Chlamydia*-like organisms, such as *Parachlamydia acanthamoebae*, *Simkania negevensis* and *Waddlia chondrophila* grow in similar vacuoles in amoebae and cells of higher animals (Everett, 2000). Similar to *Legionella pneumophila* and *Brucella abortus*, *C. trachomatis* uses host cell Golgi- and/or ER-derived vesicles to generate specialised membrane-bound compartments for the replication. We previously showed that *Simkania* establishes novel ER interaction sites at which the SnCV is extended along the ER within 3 days post infection (Mehlitz *et al*., 2014). It is likely that *Simkania* uses host cell Golgi- and/or ER-derived lipids and vesicles to generate the SnCV compartment.

Positive-strand RNA viruses are known to remodel intracellular membranes to create mini-organelles where RNA amplification and virion assembly take place (Miller and Krijnse-Locker, 2008). Flaviviruses like dengue virus and West Nile virus have been shown to replicate within membrane invaginations originating from the ER (Welsch *et al*., 2009; Gillespie *et al*., 2010). Hepatitis C virus most likely uses specialised vesicles for RNA replication that are derived primarily from the rough ER, early and late endosomes, COP vesicles, mitochondria and lipid droplets (Romero-Brey *et al*., 2012). We identified analogue cellular components in the proteome data indicating that vacuole formation processes are similar for *Simkania*. Interestingly, most proteins identified here are part of clathrin and COPI vesicle transport pathways (retrograde) that were enriched during infection whereas most exocytic and endosomal as well as COPII or other ER to Golgi transport proteins (anterograde) were depleted. This was the first hint that retrograde transport plays an important role in SnCV formation. Additionally, silencing COPB2 (COPI) and AP2B1 (clathrin) expression reduced the production of *Simkania* infectious progeny.

We demonstrated here a strong effect of Retro compounds on SnCV maturation and *Simkania* development. These inhibitors have initially been identified as compounds that prevented the cytotoxic effect of toxins that are transported via the retrograde route (Stechmann *et al*., 2010; Ming *et al*., 2013; Noel *et al*., 2013). Although the exact molecular targets of these compounds have not been identified yet, it is likely that the retrograde transport

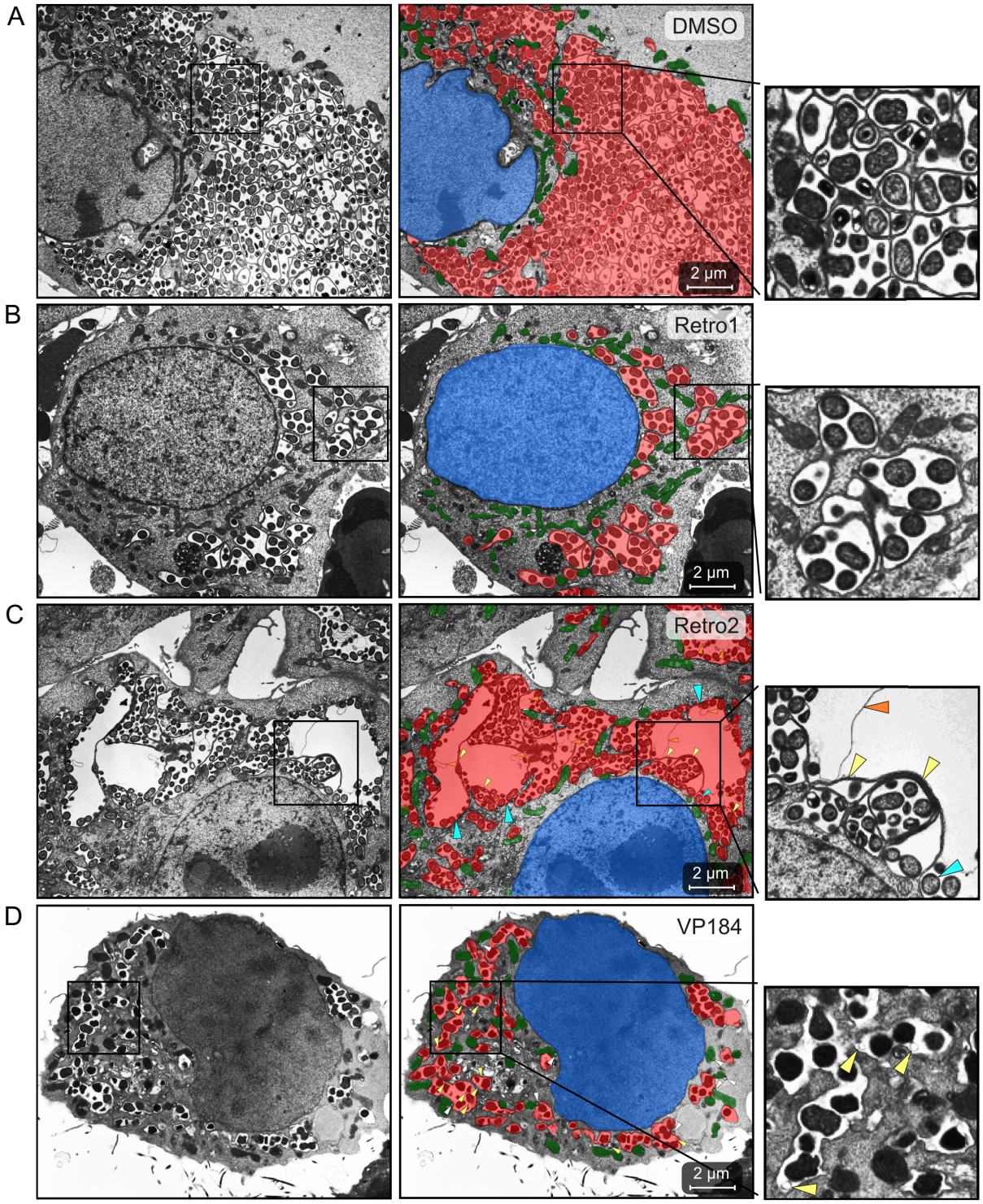

Fig. 5. Effects of Retro compounds on SnCV formation during *Simkania* infection. Transmission electron microscopy of HeLa229 cells 3 days post infection. Cells were treated with 75 µM DMSO, Retro-1, -2 and 25 µM VP-184 during infection. The SnCV (red) (Bravo *et al.*), associated to mitochondria (green) (Kahane *et al.*), spreads the cytoplasm near the nucleus (blue). A. The DMSO control shows a normal SnCV highly filled with bacteria that are covered with mitochondria. B. Retro-1 seems to affect SnCV size indicated by fewer small sub-vacuoles. C. Retro-2 seems to affect SnCV morphology and bacteria replication. Sub-vacuoles that are highly enlarged contain just few bacteria that are located at the SnCV boundary (blue arrows) and/or contain excessive membrane material (orange arrows). Some sub-vacuoles are surrounded by multiple membranes (yellow arrows). In total, the SnCV appears to be bigger in size. D. VP-184 affects cell development and SnCV size. Sub-vacuoles contain freestanding transparent vesicles of unknown origin (yellow arrows). Some mitochondria are associated with transparent droplets of unknown origin (white arrows).

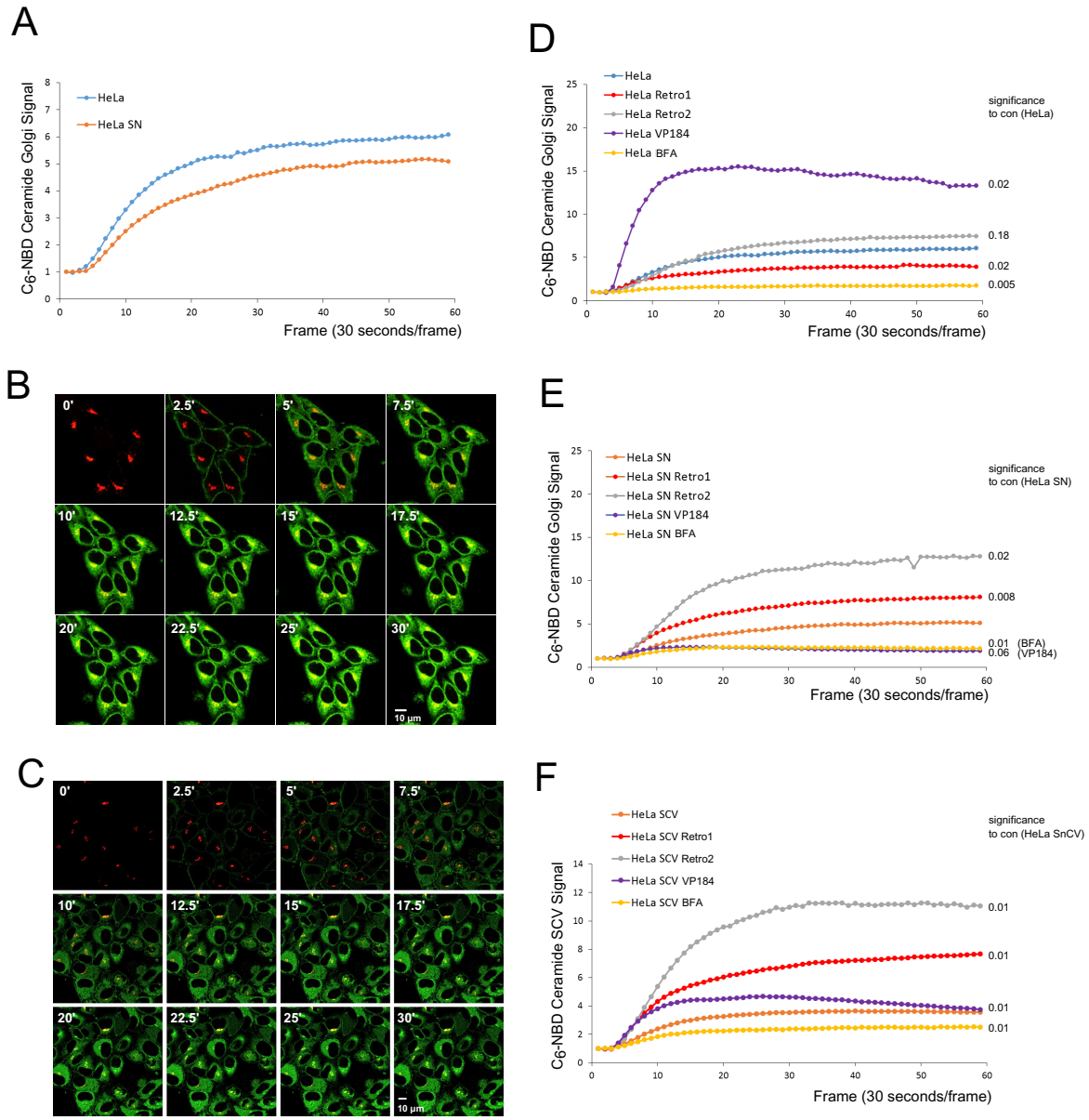

Fig. 6. Effects of Retro compounds on Golgi-dependent sphingomyelin transport to the SnCV. Time-courses of life cell imaging from intracellular C_6-NBD-ceramide transport in *Simkania*-infected or control HeLa Golgi-mRFP cells are shown. (A, D–E) Calculation of fluorescence intensity of C_6-NBD-ceramide trafficking to the Golgi apparatus and (F) to the SnCV within 30 min (2 images/frame). Curves are representative of $n = 3$ biological experiments and $m \geq 20$ cells/experiment. (B–C) Time-course images of C_6-NBD-ceramide transport in untreated *Simkania*- and non-infected HeLa cells. Red = Golgi; green = C_6-NBD-ceramide. Brefeldin A = BFA. Images are representative of $n = 3$ independent experiments.

A. C_6-NBD-ceramide transport to the Golgi rises exponentially. *Simkania*-infected cells (orange) absorb more slowly and less of the fluorescent ceramide compared to non-infected cells (blue). The maximum gain is reached at around 28–30 min.

B. Time-course images of C_6-NBD-ceramide transport in non-infected cells. Images of 2.5 min time lags starting at 0 min are illustrated.

C. Time-course images of C_6-NBD-ceramide transport in *Simkania*-infected cells. Images of 2.5 min time lags starting at 0 min are illustrated.

D. C_6-NBD-ceramide to Golgi transport in non-infected and Retro compound-, BFA- or untreated cells was analysed. Inhibitors were added 30 min prior to imaging (for more details, see *Experimental procedures* section). VP-184-treated cells (violet) showed a high increase that slightly dropped down at 12–13 min. Retro-2-treated cells (grey) showed a slight increase compared with the control (blue). Retro-1-treated cells (red) (Bravo *et al.*) showed a slight decrease. In BFA-treated cells (yellow) the transport was really weak.

E. C_6-NBD-ceramide to Golgi transport in *Simkania*-infected and Retro compound-, BFA- or untreated cells was analysed. In Retro-1- and -2-treated cells (red, grey) the fluorescent lipid transport to the Golgi was highly increased. In VP-184 and BFA-treated cells (violet, yellow), the transport was weaker but still detectable.

F. C_6-NBD-ceramide to SnCV transport in *Simkania*-infected and Retro compound-, BFA- or untreated cells was analysed. In Retro-1- and -2-treated cells (red, grey) the fluorescent lipid transport to the SnCV was highly increased. VP-184-treated cells (violet) showed a slight increase that dropped down nigh the *Sn*-control (orange). In BFA-treated cells (yellow) the transport was weaker but still detectable.

is already blocked early at the level of endosomal to TGN trafficking. We showed that Retro compounds influence intracellular SnCV formation and *Simkania* development. Electron microscopy studies indicated a strong effect on the SnCV morphology that appears to be unique for every compound. This diversity may reflect the inhibition of different targets by Retro compounds and – in line with this assumption – also different pathways of vesicular transport that all are required for SnCV formation.

In the process of inclusion formation, *Chlamydiae* actively interrupt the classical endocytic pathway very early (Scidmore *et al*., 1996a) and enter the cells' exocytic pathway that remains poorly defined (Hackstadt *et al*., 1995; 1997; Rzomp *et al*., 2003). In this study, we concentrated on retrograde trafficking as proteins controlling clathrin vesicle and COPI-Golgi to ER transport appeared enriched during *Simkania* infection. Retrograde transport involves proteins and lipids that initially are transported back from the PM and endosomes to the Golgi apparatus. Recycling endosomes serve here as a sorting organelle for retrograde transport (Bonifacino and Rojas, 2006). Subsequently proteins and lipids are transported within the TGN to the ER (Sandvig and van Deurs, 2005), which is mediated by COPI vesicles (Orci *et al*., 1997). Many viruses use similar routes to the ER for their assembly (Brandenburg and Zhuang, 2007). Recently, it was reported that Retro-2 can inhibit retrograde transport of polyoma-, papilloma- and adeno-associated viruses suggesting an overlap in the host factors used by bacterial toxins and viruses (Nelson *et al*., 2013; Carney *et al*., 2014; Nonnenmacher *et al*., 2015). Our data using Retro compounds and RNA interference during *Simkania* infection support that the SnCV is dependent on retrograde transport. It is likely that retrograde transport is required for nutrient acquisition during *Simkania* infection. Therefore, compounds like Retro-1 or -2 might be useful to hinder infection by *Simkania* and maybe *Chlamydia* as well, as they also require early endosome-to-Golgi and Golgi to ER transport for infection.

Metabolite delivery to the SnCV appears to be one of the processes that are influenced by Retro-1 and -2. Treatment with Retro-1 and -2 increased the amount of C_6-NBD-ceramide in the Golgi and the SnCV, probably due to the interference of both inhibitors with the transport of C_6-NBD-ceramide from the TGN, which could result in retention in the Golgi and increased uptake by the SnCV. VP-184 had the most dramatic effect by causing strong retention in the Golgi only in non-infected cells and blocked C_6-NBD-ceramide transport to the Golgi after infection. In infected cells, the effect of VP-184 was similar to BFA, a Golgi-disrupting compound, and lipid accumulation in the Golgi was not detected at all, pointing to an infection-dependent block of lipid transport at the Golgi under these conditions. C_6-NBD-ceramide transport to the SnCV seemed to be affected by this block at later time points. The finding that BFA prevented accumulation of C_6-NBD-ceramide in both the Golgi and the SnCV adverts to a role of the Golgi in lipid transport to the SnCV.

The chlamydial inclusion is not permeable to molecules as small as 520 Daltons (Heinzen and Hackstadt, 1997) and therefore, all larger metabolites and proteins have to cross the membrane barrier either by direct transport or by delivery via vesicle involving both human and bacteria proteins in the inclusion membrane. We used C_6-NBD-ceramide, a vital stain for the Golgi apparatus that has been used to study sphingolipid trafficking in viable cells (Lipsky and Pagano, 1985a,b; Pagano *et al*., 1989; Rosenwald and Pagano, 1993; Zhong *et al*., 2001). Within the *cis* or *medial* Golgi apparatus, C_6-NBD-ceramide is processed to sphingomyelin (SM) or glucosylceramide, like endogenous ceramide (Lipsky and Pagano, 1985a), and delivered to the PM by a vesicle-mediated pathway. By interruption of exocytic lipid transport, *C. trachomatis* (Scidmore *et al*., 1996b), *C. psittaci* (Rockey *et al*., 1996) and *C. pneumoniae* (Wolf and Hackstadt, 2001) intercept the fluorescent SM that subsequently is incorporated into the cell wall of the intracellular bacteria. This modification of intracellular lipid trafficking by induced fusion of the inclusion with a subset of exocytic vesicles leads to the acquisition of a significant amount of the exported SM (Fields and Hackstadt, 2002). *Simkania* like other *Chlamydia* species (Fritsche *et al*., 2000) lack genes for SM biosynthesis and therefore likely intercept SM by exploiting the host cell ceramide transport. Prolonged treatment with BFA causes disassembly of the Golgi apparatus and induces redistribution of Golgi, secretory and membrane proteins into the ER. BFA has been shown to abrogate SM transport to the chlamydial inclusion (Scidmore *et al*., 1996b). We observed that BFA generally blocks C_6-NBD-ceramide uptake, indicating an early inhibition of ceramide transport already at the PM. Despite advanced Golgi fragmentation in BFA-treated cells, small amounts of ceramide were incorporated into the SnCV, suggesting that *Simkania* gains the main part of ceramide directly from the Golgi but uses also other pathways for lipid acquisition. The enhanced accumulation of ceramide in the SnCV could be directly stimulated by the blocked transport to or out of the Golgi (treatment with Retro-1, Retro-2, perhaps also VP-184) resulting in increased transfer of ceramide to other transport pathways, e.g. clathrin-derived vesicles. This is supported by similar findings on retrograde toxin transport in Vero cells (Schapiro *et al*., 1998) as well as enrichment of clathrin-associated proteins like AP2A1 and AP2B1 found in our LC-MS^2 analysis. BFA treatment has no effect on *Chlamydia* replication (Scidmore *et al*., 1996b), suggesting that *C. trachomatis* acquires SM by additional routes that involve BFA-insensitive and/or non-vesicular trafficking pathways

(Derre *et al*., 2011; Elwell *et al*., 2011; Dumoux *et al*., 2012). These may involve bacterial effector proteins as in case of *Salmonella*, where the SPI-2 effector SseL binds to a lipid-binding protein and may direct host lipid-transport to the *Salmonella*-containing vacuole (Auweter *et al*., 2012).

We show here that early events in retrograde transport seem to be essential for SnCV formation, *Simkania* development and ceramide acquisition. Because we do not know the targets of the Retro compounds, the affected trafficking pathways remain to be defined. We cannot exclude COPI-dependent and independent pathways of retrograde transport, the ERGIC as first anterograde and retrograde sorting station or the influence of depleted anterograde transport proteins during infection. We hypothesise that the enrichment of clathrin or Golgi to ER transported proteins in addition to the depletion of many anterograde transported proteins indicates a direct bypass of important nutrient trafficking pathways to the SnCV during infection. Further studies are necessary to understand the influence of retrograde and anterograde transport on *Simkania* development.

Experimental procedures

Cell lines and bacteria

HeLa229 (ATCC CCL-2.1) were grown in RPMI1640 medium (Glutamax, 10% FBS, w/o HEPES) (Invitrogen). Stable HeLa229 cell lines were established to constantly label the Golgi apparatus (B4GalT1 in a pCMV6-AC-mRFP cloning vector, OriGene) and the ER (KDEL in a pDsRed2-ER expression vector). Selection for B4GalT1-mRFP or KDEL-DsRed2 was done with G418 (400 μg/ml). *S. negevensis* strain Z (ATCC VR-1471) was prepared as described previously (Mehlitz *et al*., 2014). Briefly, HeLa229 cells were grown to 50–70% confluence and were inoculated with *S. negevensis* in RPMI1640 with 5% FBS, for 6 h at 35°C in a humidified incubator at 5% CO_2. Medium was replaced by infection medium (RPMI1640, Glutamax, 5% FBS, w/o HEPES), and growth was allowed for 3 days. Cells were mechanically detached, and bacteria were released using ~ 2–5 mm glass beads (Carl Roth). Low speed supernatant (600 × *g*, 4°C and 5 min) was subjected to high-speed centrifugation (20 000 × *g*, 4°C and 30 min) to pellet bacteria. Bacteria were washed twice with 5 ml SPG (250 mM sucrose, 50 mM sodium phosphate, 5 mM glutamate, pH 7.4), aliquoted and stored at –80°C in SPG.

ER-SnCV purification

HeLa229 cells were seeded in 6-well cluster plates (12 plates/experiment) and grown to 70% confluence before infection with *Simkania* at multiplicity of infection (moi) 1.0 (see also Fig. 1A for experimental scheme). Plates were centrifuged for 1 h at 4°C, 910 × *g* and inoculated for 5 h at 35°C in a humidified incubator at 5% CO_2. Medium was replaced by infection medium and growth was allowed for 3 days. Growth medium was removed, and cells were released with a rubber policeman into ice-cold PBS followed by one wash step ice cold PBS (5 min, 4°C, 600 × *g*). PBS was replaced by 600 μl 0.5 × hypotonic buffer (10 mM HEPES, 0.5 mM EGTA, 12.5 mM KCl, 0.125 M sucrose, protease and phosphatase inhibitors, pH 7.6), and cells were incubated for 20 min at 4°C in a rotary shaker. Cells were pelleted (5 min, 4°C, 600 × *g*) and resuspended in 0.5 × isotonic buffer (5 mM HEPES, 0.5 mM EGTA, 12.5 mM KCl, protease and phosphatase inhibitors, pH 7.6) and sonicated at 4°C for 10 min in a sonication bath. Prelysate was homogenised with a Dounce Homogenizer (glass cylinder and pestle), 10 strokes at 200 r.p.m. Crude microsomal fraction containing ER and SnCV were prepared by sequential centrifugation: (i) pre-nuclear fraction (PNF) – 1,000 × *g* at 4°C for 10 min; (ii) pre-mitochondrial fraction (PMF) – 12 000 × *g* at 4°C for 15 min and (iii) crude microsomal fraction (CMF) – 100 000 × *g* at 4°C for 1 h in an Optima MAX-XP ultra-centrifuge using a MLA-80 fixed angle rotor (Beckmann Coulter).

Reagents and antibodies

Chemicals were obtained from Sigma-Aldrich (Germany) unless otherwise stated. Primary antibodies used: Calnexin (Cell Signaling, C5C9), PDI (Cell Signaling, C81H6), ERp72 (Cell Signaling, D70D12), KDEL (Enzo, 10C3), Lamin B1 (Santa Cruz, 6216), Sam50 (kindly provided by Vera Kozjak-Pavlovic), β-Actin (Sigma-Aldrich, A5441), CCT2 (Cell Signaling, 3561), GEF H1 (55B6) (Cell Signaling, 4076), VDAC1 (Calbiochem, 529532), TOMM40 (Santa Cruz, sc-11414) and VAMP2 (D601A) (Cell Signaling, 13508). Antibodies against GroEL (anti-*Sn*-GroEL) or whole bacteria (anti-*Simkania*) were prepared as previously described (Mehlitz *et al*., 2014). Carbocyanine-labelled secondary antibodies were purchased from Dianova. Nuclear staining was done with 4', 6-diamidino-2-phenylindole (DAPI). Fluorescent sphingolipid NBD-C_6-ceramide (6 – ((N – [7 – nitrobenz – 2 – oxa – 1, 3 – diazol – 4 – yl) amino) hexanoyl] sphingosine) complexed to BSA was obtained from Molecular Probes (Invitrogen, N-1154). G418 was obtained from InvivoGen. Protease and phosphatase inhibitors were obtained from Roche.

Immunoblotting and immunofluorescence staining

Western blotting was performed according to standard procedures (Mehlitz *et al*., 2010), and signals were detected with a Chemo Cam Imager (Intas). Quantification was performed using FIJI (ImageJ) and Excel (Microsoft). For immunofluorescence, cells were seeded in 12-well cluster plates with or without coverslips and were infected in a humidified incubator at 35°C and 5% CO_2 with mois indicated in the respective experiments. Cells were fixed at indicated time points with 4% PFA-sucrose for 25 min, washed once with PBS and stained while gently shaking. Subsequently cells were permeabilised with 0.2% Triton X-100 in PBS for 45 min and washed 3 × with PBS for 15 min at RT. Cells were blocked with 2% goat serum in PBS for 60 min and were stained with primary antibodies diluted in 2% goat serum in PBS for 24 h at 4°C. After 3 × washing with PBS for 15 min, samples were incubated with secondary antibodies for 1 h in blocking solution at RT in the dark. Cells were washed 3 × with PBS and counterstained with DAPI (1 μg/ml) in PBS for 15 min. Cov-

Table 1. Non-linear gradient operating parameters for peptide elution.

Duration (Ming *et al.*)	% B (final)
5	1
120	25
30	50
1	99
5	99
1	1
18	1

erslips were mounted with Mowiol 4–88 (Carl Roth) after short wash with H_2O. The 12-well cluster plates without coverslips were washed 3 × with PBS for 15 min and visualised at RT. Samples were subsequently viewed on either a Leica DMIR or TCS SP5 microscope (Leica Microsystems GmbH, Wetzlar, Germany), respectively. Data were processed using FIJI (ImageJ) (http://fiji.sc/) (Laboratory for Optical and Computational Instrumentation (LOCI), University of Wisconsin-Madison, USA).

Electron microscopy

Samples were fixed with 2.5% glutaraldehyde (50 mM sodium cacodylate pH 7.2; 50 mM KCl; 2.5 mM $MgCl_2$) at 4°C for 1 h and buffered with 50 mM sodium cacodylate (pH 7.2) at 4°C. Then samples were incubated with OsO_4 for 2 h at 4°C. Cells were dehydrated, embedded in Epon812 and ultrathin sectioned at 50 nm. Sections were stained with 2% uranyl acetate in ethanol, followed by staining with lead citrate and analysed on a Zeiss EM10 (Zeiss, Germany).

LC-MS/MS

For LC-MS^2 measurements, three biological replicates of ER-SnCV purified samples were generated and analysed. Proteins were separated by 1D-SDS-PAGE, the gel lanes were excised in 10 equidistant pieces and subjected to trypsin digestion as described before (Otto *et al.*, 2010). For LC-MS/MS analyses, in-house self-packed columns were prepared and used with an EASY-nLC II system (Thermo). In brief fused silica emitter tips with an inner diameter of 100 μm and an outer diameter of 360 μm were prepared by using a P-2000 laser puller (Sutter Instruments, Novato, CA). The resulting emitter tip was then packed with Phenomenex Aeris C18 reversed phase material (3.6 μm particles) in custom build pressure bomb to obtain a 20 cm nano-LC column.

The peptides were loaded onto the column with 10 μl buffer A (0.1% acetic acid) at a constant flow rate of 500 nl/min without trapping. Subsequently, peptides were eluted using a non-linear 180 min gradient from 1% to 99% buffer B (0.1% acetic acid in acetonitrile) with a constant flow rate of 300 nl/min and injected online into the mass spectrometer. Voltages between the emitter capillary and the orifice were set to 2.5 kV by using liquid junction. Afterward, the column was washed with 99% buffer B for 5 min and equilibrated with 99% buffer A for 18 min. The gradient is described in Table 1.

MS and MS/MS data were acquired with a LTQ Orbitrap Classic (Thermo). After a survey scan at a resolution of R = 30 000 within a scan range (m/z) of 300–2000 in the Orbitrap with activated lockmass correction, the five most abundant precursor ions were selected for fragmentation. Singly charged ions as well as ions without detected charge states were not selected for MS/MS analysis. CID fragmentation was performed for 30 ms with normalised collision energy of 35, and the fragment ions were recorded in the linear ion trap.

After mass spectrometric measurement, MS data were subjected to database searching via Sorcerer using Sequest (version 27, revision 11; SageN, Milptas, CA, USA) without charge state deconvolution and deisotoping performed. Database searching was performed with a database of combined entries of NCBI *Simkania negevensis* NC 015713 and NC 015710 and UniProtKB *Homo sapiens* (version 2/12). The combined database was used as target/decoy databases with a list of common contaminants added (45580 entries). Sequest was used assuming trypsinisation with a fragment ion mass tolerance of 1.00 Da and a search tolerance of 10 ppm for the overview scans. Oxidation of methionine was specified in Sequest as a variable modification. Scaffold (version 3.5.1, Proteome Software, Portland, OR, USA) was used to filter and validate MS/MS-based peptide and protein identifications. Peptide identifications were accepted when spectra exceeded Xcorr values of 2.2, 3.3 and 3.8 for doubly, triply and quadruply charged peptides with deltaCN values of more than 0.1. Protein identifications are based on at least 2 unique peptides. Proteins that contained similar peptides and could not be differentiated based on MS/MS analysis alone were grouped to meet the principle of parsimony.

Analysis of proteomics data

Proteomics data were analysed via Web-based Gene SeT AnaLysis Toolkit (WEBGestalt) (Wang *et al.*, 2013). Enrichment analysis was performed using GO Analysis against the *Homo sapiens* genome. WEBGestalt settings were hypergeometric statistical method and multiple test adjustment according to Benjamini and Hochberg (1995). Significance levels allowed only the top 10 categories at a minimum protein number of 10 per category. Proteomic count data was filtered using Scaffold as described above (LC-MS/MS). Differential expression was analysed using the edgeR method (Robinson *et al.*, 2010) as implemented in the statistical package msmsTest (Gregori *et al.*, 2013) in the software R. Given the uncertainty of normalisation factor estimation due to the relatively small in number and possibly selected set of proteins detected we did not normalise counts across samples by default. Estimated normalisation factors for paired samples showed that those were rather small (< 0.1-fold difference for all pairs). We used a model incorporating each experiment as blocking factor to perform paired tests. As a sensitivity analysis, we repeated the analysis using edgeR's global normalisation method, which resulted in the same list of differentially expressed genes (adjusted $P < 0.2$) except for proteins HNRPC, K1C18, K2C8, SFXN1, AHNK, PABP1, ATPO and SEPT2. Heatmaps were generated after a variance stabilising transformation as provided by package DESeq (Love *et al.*, 2014), adjusting for experiment effects using the same model

as above. Trafficking proteins were further analysed via 'Search Tool for the Retrieval of INteracting Genes/proteins' (STRING) (von Mering *et al*., 2003) allowing standard setting for predictive methods (Neighbourhood, Gene Fusion, Co-occurrence, Co-expression, Experiments, Databases and Textmining) at medium confidence (0.4).

Infectivity assays

The 40 000 cells were seeded in 12-well cluster plates, inhibitor-treated and infected as indicated in the respective experiment. Cells were processed for immunoblotting, immunofluorescence staining or infectivity assay. For infectivity assays cells were either fixed and stained at indicated time points (inclusion formation/primary infection) or bacteria were released via one freeze thaw cycle (–70°C/37°C) followed by mechanical release through pipetting and transfer to fresh HeLa229 cells (1:25–1:50, progeny/infectivity). Cells were centrifuged for 1 h at 35°C and medium exchanged to infection medium. Progeny was fixed at day 3 post infection and processed for staining or harvested for immunoblotting. Infectivity assays were imaged on an automated fluorescence microscope Leica DMIR. Numbers and average sizes of the SnCV as well as host cell numbers were determined via GroEL and DAPI staining, and images were analysed and quantified using FIJI (ImageJ) and Excel (Microsoft).

siRNA transfections

SiRNA against STX5 (GS6811), COPB2 (GS9276), AP2B1 (GS163), All-Stars negative control (SI03650325) were purchased from Qiagen. ARHGEF2 siRNA was obtained from Dharmacon (M-009883-01-0005). Transfection was done using HiPerFect transfection reagent (301705) as described in the manufacturer's instructions (Qiagen).

RNA isolation and qRT-PCR

RNA was isolated using TRI reagent solution (Ambion, AM9738) according to manufacturer's instructions. Instead of BCP, we used 200 µl chloroform. Total RNA concentration was determined by using a NanoDrop fluorospectrometer (Thermo Scientific). Synthesis of first strand cDNA was performed on 1–2 µg total RNA by using RevertAid RT Reverse Transcription Kit (Thermo Fisher, K1691). QRT-PCR was performed on 20 µl reaction volumes in triplicates using SYBR green master mix (Quanta, 733–1386) according to the manufacturer's instructions. qRT-PCRs were performed on a StepOnePlus instrument (Applied Biosystems, 96 wells), and data were analysed using the $\Delta\Delta C_T$ – method and StepOne software v2.3 (Applied Biosystems). Primers used were AP2B1: 5′-CCAGAGCATTGATGTCTCCC-3′ (F), 5′-GGGATGAGGCAGCTGAAGTA-3′ (R); ARHGEF2: 5′-CTCGAAAGAAAGTTGCTCCG-3′ (F), 5′-ACAGGCATAGCACATGGTCA-3′ (R); COPB2: 5′-GTAGCCGGTAACAAACGAGG-3′ (F), 5′-CCAACATCCATGGCTCTGTA-3′ (R); STX5: 5′-TGAGTTGGGCTCCATCTTTC-3′ (F), 5′-TTGAGGATCTCTGAATGGGC-3′ (R).

C_6-NBD-ceramide labelling and life cell imaging

The 100,000–150,000 cells were seeded in ibidi µ-dishes, 35 mm, high (Ibidi). Cells were infected with *S. negevensis* for 6 h at 35°C in a humidified incubator at 5% CO_2. Medium was replaced by infection medium, and growth was allowed for 3 days. Medium was exchanged 30 min prior to imaging with PBS and 1 ml of pre-warmed RPMI1640 medium (Glutamax, w/o FCS, 25 mM HEPES, w/o phenol red) containing inhibitors at following concentrations: 0.2 µg/ml BFA, 25 µM VP-183, 75 µM Retro-1 or 75 µM Retro-2. For imaging, cells were transferred to a pre-warmed microscopy chamber mounted to a Leica TCS SP5 microscope. µ-dishes were imaged without lid and after focusing cells were initially imaged 2 min for system stability (two images/minute). Experiments were started adding 10 µl of 50 µM C_6-NBD-ceramide in PBS to the pre-focused cells, and imaging was allowed to proceed for at least 28 min at two images per minute. Ceramide uptake was quantified by setting a region of interest around the Golgi or within the SnCV and measuring the C_6-NBD intensity using ImageJ. C_6-NBD uptake in the respective area was normalised to C_6-NBD intensity at time point $t = 0$. Intensity ratios were calculated with Excel (Microsoft).

Acknowledgements

We thank Claudia Binder, Andrea Fick, Nadine Vornberger, Daniela Bunsen, Claudia Gehrig and Sebastian Grund for excellent technical assistance. We thank Jean-Christophe Cintrat (iBiTec-S, SCBM, France) and Daniel Gillet (iBiTec-S, SIMOPRO, France) for providing the retrograde transport inhibitors. We thank Andreas Demuth for critical reading of the manuscript. This work was supported by the DFG priority program SPP1580 to T.R., J.B. and V.P. were supported by the French National Agency for Research (ANR) under Contract ANR-11-BSV2-0018 RETROscreen, the Joint ministerial program of R&D against CBRNE risks and CEA.

References

Aeberhard, L., Banhart, S., Fischer, M., Jehmlich, N., Rose, L., Koch, S., *et al*. (2015) The proteome of the isolated *Chlamydia trachomatis* containing vacuole reveals a complex trafficking platform enriched for retromer components. *PLoS Pathog* **11:** e1004883.

Al-Younes, H.M., Rudel, T., and Meyer, T.F. (1999) Characterization and intracellular trafficking pattern of vacuoles containing *Chlamydia pneumoniae* in human epithelial cells. *Cell Microbiol* **1:** 237–247.

Anderson, T.D., and Cheville, N.F. (1986) Ultrastructural morphometric analysis of *Brucella abortus*-infected trophoblasts in experimental placentitis. Bacterial replication occurs in rough endoplasmic reticulum. *Am J Pathol* **124:** 226–237.

Auweter, S.D., Yu, H.B., Arena, E.T., Guttman, J.A., and Finlay, B.B. (2012) Oxysterol-binding protein (OSBP) enhances replication of intracellular *Salmonella* and binds the *Salmonella* SPI-2 effector SseL via its N-terminus. *Microbes Infect* **14:** 148–154.

Babia, T., Ledesma, M.D., Saffrich, R., Kok, J.W., Dotti, C.G.,

and Egea, G. (2001) Endocytosis of NBD-sphingolipids in neurons: exclusion from degradative compartments and transport to the Golgi complex. *Traffic* **2:** 395–405.

Beatty, W.L. (2006) Trafficking from CD63-positive late endocytic multivesicular bodies is essential for intracellular development of *Chlamydia trachomatis*. *J Cell Sci* **119:** 350–359.

Beatty, W.L. (2008) Late endocytic multivesicular bodies intersect the chlamydial inclusion in the absence of CD63. *Infect Immun* **76:** 2872–2881.

Benjamini, Y., and Hochberg, Y. (1995) Controlling the false discovery rate: a practical and powerful approach to multiple testing. *J R Stat Soc Ser B* **57** (1)**:** 289–300.

Bonifacino, J.S., and Glick, B.S. (2004) The mechanisms of vesicle budding and fusion. *Cell* **116:** 153–166.

Bonifacino, J.S., and Rojas, R. (2006) Retrograde transport from endosomes to the trans-Golgi network. *Nat Rev Mol Cell Biol* **7:** 568–579.

Braakman, I., and Bulleid, N.J. (2011) Protein folding and modification in the mammalian endoplasmic reticulum. *Annu Rev Biochem* **80:** 71–99.

Brandenburg, B., and Zhuang, X. (2007) Virus trafficking – learning from single-virus tracking. *Nat Rev Microbiol* **5:** 197–208.

Brandizzi, F., and Barlowe, C. (2013) Organization of the ER-Golgi interface for membrane traffic control. *Nat Rev Mol Cell Biol* **14:** 382–392.

Bravo, R., Parra, V., Gatica, D., Rodriguez, A.E., Torrealba, N., Paredes, F., *et al*. (2013) Endoplasmic reticulum and the unfolded protein response: dynamics and metabolic integration. *Int Rev Cell Mol Biol* **301:** 215–290.

Breckenridge, D.G., Germain, M., Mathai, J.P., Nguyen, M., and Shore, G.C. (2003) Regulation of apoptosis by endoplasmic reticulum pathways. *Oncogene* **22:** 8608–8618.

Carabeo, R.A., Mead, D.J., and Hackstadt, T. (2003) Golgi-dependent transport of cholesterol to the *Chlamydia trachomatis* inclusion. *Proc Natl Acad Sci USA* **100:** 6771–6776.

Carney, D.W., Nelson, C.D., Ferris, B.D., Stevens, J.P., Lipovsky, A., Kazakov, T., *et al*. (2014) Structural optimization of a retrograde trafficking inhibitor that protects cells from infections by human polyoma- and papillomaviruses. *Bioorg Med Chem* **22:** 4836–4847.

Clausen, J.D., Christiansen, G., Holst, H.U., and Birkelund, S. (1997) *Chlamydia trachomatis* utilizes the host cell microtubule network during early events of infection. *Mol Microbiol* **25:** 441–449.

Collingro, A., Tischler, P., Weinmaier, T., Penz, T., Heinz, E., Brunham, R.C., *et al*. (2011) Unity in variety – the pan-genome of the *Chlamydiae*. *Mol Biol Evol* **28:** 3253–3270.

Dautry-Varsat, A., Subtil, A., and Hackstadt, T. (2005) Recent insights into the mechanisms of *Chlamydia* entry. *Cell Microbiol* **7:** 1714–1722.

Derre, I., Swiss, R., and Agaisse, H. (2011) The lipid transfer protein CERT interacts with the *Chlamydia* inclusion protein IncD and participates to ER-Chlamydia inclusion membrane contact sites. *PLoS Pathog* **7:** e1002092.

Desjardins, M. (2003) ER-mediated phagocytosis: a new membrane for new functions. *Nat Rev Immunol* **3:** 280–291.

Dumoux, M., Clare, D.K., Saibil, H.R., and Hayward, R.D. (2012) *Chlamydiae* assemble a pathogen synapse to hijack the host endoplasmic reticulum. *Traffic* **13:** 1612–1627.

Elwell, C.A., Jiang, S., Kim, J.H., Lee, A., Wittmann, T., Hanada, K., *et al*. (2011) *Chlamydia trachomatis* co-opts GBF1 and CERT to acquire host sphingomyelin for distinct roles during intracellular development. *PLoS Pathog* **7:** e1002198.

English, A.R., Zurek, N., and Voeltz, G.K. (2009) Peripheral ER structure and function. *Curr Opin Cell Biol* **21:** 596–602.

Everett, K.D. (2000) *Chlamydia* and *Chlamydiales*: more than meets the eye. *Vet Microbiol* **75:** 109–126.

Everett, K.D., Bush, R.M., and Andersen, A.A. (1999) Emended description of the order *Chlamydiales*, proposal of *Parachlamydiaceae* fam. nov. and *Simkaniaceae* fam. nov., each containing one monotypic genus, revised taxonomy of the family *Chlamydiaceae*, including a new genus and five new species, and standards for the identification of organisms. *Int J Syst Bacteriol* **49** (Part 2): 415–440.

Fields, K.A., and Hackstadt, T. (2002) The chlamydial inclusion: escape from the endocytic pathway. *Annu Rev Cell Dev Biol* **18:** 221–245.

Friis, R.R. (1972) Interaction of L cells and *Chlamydia psittaci*: entry of the parasite and host responses to its development. *J Bacteriol* **110:** 706–721.

Fritsche, T.R., Horn, M., Wagner, M., Herwig, R.P., Schleifer, K.H., and Gautom, R.K. (2000) Phylogenetic diversity among geographically dispersed *Chlamydiales* endosymbionts recovered from clinical and environmental isolates of *Acanthamoeba* spp. *Appl Environ Microbiol* **66:** 2613–2619.

Ghaemmaghami, S., Huh, W.K., Bower, K., Howson, R.W., Belle, A., Dephoure, N., *et al*. (2003) Global analysis of protein expression in yeast. *Nature* **425:** 737–741.

Gillespie, L.K., Hoenen, A., Morgan, G., and Mackenzie, J.M. (2010) The endoplasmic reticulum provides the membrane platform for biogenesis of the flavivirus replication complex. *J Virol* **84:** 10438–10447.

Gregori, J., Villarreal, L., Sanchez, A., Baselga, J., and Villanueva, J. (2013) An effect size filter improves the reproducibility in spectral counting-based comparative proteomics. *J Proteomics* **95:** 55–65.

Grieshaber, S.S., Grieshaber, N.A., and Hackstadt, T. (2003) *Chlamydia trachomatis* uses host cell dynein to traffic to the microtubule-organizing center in a p50 dynamitin-independent process. *J Cell Sci* **116:** 3793–3802.

Hackstadt, T. (2000) Redirection of host vesicle trafficking pathways by intracellular parasites. *Traffic* **1:** 93–99.

Hackstadt, T., Scidmore, M.A., and Rockey, D.D. (1995) Lipid metabolism in *Chlamydia trachomatis*-infected cells: directed trafficking of Golgi-derived sphingolipids to the chlamydial inclusion. *Proc Natl Acad Sci USA* **92:** 4877–4881.

Hackstadt, T., Fischer, E.R., Scidmore, M.A., Rockey, D.D., and Heinzen, R.A. (1997) Origins and functions of the chlamydial inclusion. *Trends Microbiol* **5:** 288–293.

Hackstadt, T., Scidmore-Carlson, M.A., Shaw, E.I., and Fischer, E.R. (1999) The *Chlamydia trachomatis* IncA protein is required for homotypic vesicle fusion. *Cell Microbiol* **1:** 119–130.

Hahn, D.L., and McDonald, R. (1998) Can acute *Chlamydia pneumoniae* respiratory tract infection initiate chronic asthma? *Ann Allergy Asthma Immunol* **81:** 339–344.

Hanada, K. (2010) Intracellular trafficking of ceramide by ceramide transfer protein. *Proc Jpn Acad Ser B Phys Biol Sci* **86:** 426–437.

Hanada, K., Kumagai, K., Yasuda, S., Miura, Y., Kawano, M., Fukasawa, M., and Nishijima, M. (2003) Molecular machinery for non-vesicular trafficking of ceramide. *Nature* **426:** 803–809.

Harkinezhad, T., Geens, T., and Vanrompay, D. (2009) *Chlamydophila psittaci* infections in birds: a review with emphasis on zoonotic consequences. *Vet Microbiol* **135:** 68–77.

Heinz, E., Rockey, D.D., Montanaro, J., Aistleitner, K., Wagner, M., and Horn, M. (2010) Inclusion membrane proteins of *Protochlamydia amoebophila* UWE25 reveal a conserved mechanism for host cell interaction among the *Chlamydiae*. *J Bacteriol* **192:** 5093–5102.

Heinzen, R.A., and Hackstadt, T. (1997) The *Chlamydia trachomatis* parasitophorous vacuolar membrane is not passively permeable to low-molecular-weight compounds. *Infect Immun* **65:** 1088–1094.

Heinzen, R.A., Scidmore, M.A., Rockey, D.D., and Hackstadt, T. (1996) Differential interaction with endocytic and exocytic pathways distinguish parasitophorous vacuoles of *Coxiella burnetii* and *Chlamydia trachomatis*. *Infect Immun* **64:** 796–809.

Herweg, J.A., Hansmeier, N., Otto, A., Geffken, A.C., Subbarayal, P., Prusty, B.K., *et al*. (2015) Purification and proteomics of pathogen-modified vacuoles and membranes. *Front Cell Infect Microbiol* **5:** 48. doi:10.3389/fcimb.2015.00048.

Heuer, D., Rejman Lipinski, A., Machuy, N., Karlas, A., Wehrens, A., Siedler, F., *et al*. (2009) *Chlamydia* causes fragmentation of the Golgi compartment to ensure reproduction. *Nature* **457:** 731–735.

Horn, M. (2008) *Chlamydiae* as symbionts in eukaryotes. *Annu Rev Microbiol* **62:** 113–131.

Horwitz, M.A. (1983) Formation of a novel phagosome by the Legionnaires' disease bacterium (*Legionella pneumophila*) in human monocytes. *J Exp Med* **158:** 1319–1331.

Huber, L.A., Pfaller, K., and Vietor, I. (2003) Organelle proteomics: implications for subcellular fractionation in proteomics. *Circ Res* **92:** 962–968.

Hughes, C., Maharg, P., Rosario, P., Herrell, M., Bratt, D., Salgado, J., and Howard, D. (1997) Possible nosocomial transmission of psittacosis. *Infect Control Hosp Epidemiol* **18:** 165–168.

Hybiske, K., and Stephens, R.S. (2007) Mechanisms of host cell exit by the intracellular bacterium *Chlamydia*. *Proc Natl Acad Sci USA* **104:** 11430–11435.

Kahane, S., Gonen, R., Sayada, C., Elion, J., and Friedman, M.G. (1993) Description and partial characterization of a new *Chlamydia*-like microorganism. *FEMS Microbiol Lett* **109:** 329–333.

Kahane, S., Greenberg, D., Friedman, M.G., Haikin, H., and Dagan, R. (1998) High prevalence of '*Simkania* Z,' a novel *Chlamydia*-like bacterium, in infants with acute bronchiolitis. *J Infect Dis* **177:** 1425–1429.

Kahane, S., Everett, K.D., Kimmel, N., and Friedman, M.G. (1999) *Simkania negevensis* strain ZT: growth, antigenic and genome characteristics. *Int J Syst Bacteriol* **49** (Part 2): 815–820.

Kahane, S., Kimmel, N., and Friedman, M.G. (2002) The growth cycle of *Simkania negevensis*. *Microbiology* **148:** 735–742.

Kahane, S., Fruchter, D., Dvoskin, B., and Friedman, M.G. (2007) Versatility of *Simkania negevensis* infection in vitro and induction of host cell inflammatory cytokine response. *J Infect* **55:** e13–e21.

Karunakaran, K., Mehlitz, A., and Rudel, T. (2011) Evolutionary conservation of infection-induced cell death inhibition among *Chlamydiales*. *PLoS ONE* **6:** e22528.

Lamoth, F., and Greub, G. (2010) Amoebal pathogens as emerging causal agents of pneumonia. *FEMS Microbiol Rev* **34:** 260–280.

Lawn, A.M., Blyth, W.A., and Taverne, J. (1973) Interactions of TRIC agents with macrophages and BHK-21 cells observed by electron microscopy. *J Hyg (Lond)* **71:** 515–528.

Lieberman, D., Kahane, S., Lieberman, D., and Friedman, M.G. (1997) Pneumonia with serological evidence of acute infection with the *Chlamydia*-like microorganism 'Z'. *Am J Respir Crit Care Med* **156:** 578–582.

Lipsky, N.G., and Pagano, R.E. (1985a) Intracellular translocation of fluorescent sphingolipids in cultured fibroblasts: endogenously synthesized sphingomyelin and glucocerebroside analogues pass through the Golgi apparatus en route to the plasma membrane. *J Cell Biol* **100:** 27–34.

Lipsky, N.G., and Pagano, R.E. (1985b) A vital stain for the Golgi apparatus. *Science* **228:** 745–747.

Love, M.I., Huber, W., and Anders, S. (2014) Moderated estimation of fold change and dispersion for RNA-seq data with DESeq2. *Genome Biol* **15** (12)**:** 550. doi:10.1186/s13059-014-0550-8.

Mehlitz, A., Banhart, S., Maurer, A.P., Kaushansky, A., Gordus, A.G., Zielecki, J., *et al*. (2010) Tarp regulates early *Chlamydia*-induced host cell survival through interactions with the human adaptor protein SHC1. *J Cell Biol* **190:** 143–157.

Mehlitz, A., Karunakaran, K., Herweg, J.A., Krohne, G., van de Linde, S., Rieck, E., *et al*. (2014) The chlamydial organism *Simkania negevensis* forms ER vacuole contact sites and inhibits ER-stress. *Cell Microbiol* **16:** 1224–1243.

von Mering, C., Huynen, M., Jaeggi, D., Schmidt, S., Bork, P., and Snel, B. (2003) STRING: a database of predicted functional associations between proteins. *Nucleic Acids Res* **31:** 258–261.

Miller, S., and Krijnse-Locker, J. (2008) Modification of intracellular membrane structures for virus replication. *Nat Rev Microbiol* **6:** 363–374.

Ming, X., Carver, K., Fisher, M., Noel, R., Cintrat, J.C., Gillet, D., *et al*. (2013) The small molecule Retro-1 enhances the pharmacological actions of antisense and splice switching oligonucleotides. *Nucleic Acids Res* **41:** 3673–3687.

Mirrashidi, K.M., Elwell, C.A., Verschueren, E., Johnson, J.R., Frando, A., Von Dollen, J., *et al*. (2015) Global mapping of the Inc-human interactome reveals that retromer restricts *Chlamydia* infection. *Cell Host Microbe* **18:** 109–121.

Nelson, C.D., Carney, D.W., Derdowski, A., Lipovsky, A.,

Gee, G.V., O'Hara, B., *et al*. (2013) A retrograde trafficking inhibitor of ricin and Shiga-like toxins inhibits infection of cells by human and monkey polyomaviruses. *MBio* **4:** e729–e713.

Noel, R., Gupta, N., Pons, V., Goudet, A., Garcia-Castillo, M.D., Michau, A., *et al*. (2013) N-methyldihydroquinazolinone derivatives of Retro-2 with enhanced efficacy against Shiga toxin. *J Med Chem* **56:** 3404–3413.

Nonnenmacher, M.E., Cintrat, J.C., Gillet, D., and Weber, T. (2015) Syntaxin 5-dependent retrograde transport to the trans-Golgi network is required for adeno-associated virus transduction. *J Virol* **89:** 1673–1687.

Ojcius, D.M., Hellio, R., and Dautry-Varsat, A. (1997) Distribution of endosomal, lysosomal, and major histocompatability complex markers in a monocytic cell line infected with *Chlamydia psittaci*. *Infect Immun* **65:** 2437–2442.

van Ooij, C., Kalman, L., van Ijzendoorn, Nishijima, M., Hanada, K., Mostov, K., and Engel, J.N. (2000) Host cell-derived sphingolipids are required for the intracellular growth of *Chlamydia trachomatis*. *Cell Microbiol* **2:** 627–637.

Orci, L., Stamnes, M., Ravazzola, M., Amherdt, M., Perrelet, A., Sollner, T.H., and Rothman, J.E. (1997) Bidirectional transport by distinct populations of COPI-coated vesicles. *Cell* **90:** 335–349.

Otto, A., Bernhardt, J., Meyer, H., Schaffer, M., Herbst, F.A., Siebourg, J., *et al*. (2010) Systems-wide temporal proteomic profiling in glucose-starved *Bacillus subtilis*. *Nat Commun* **1:** 137. doi: 10.1038/ncomms1137.

Pagano, R.E., Sepanski, M.A., and Martin, O.C. (1989) Molecular trapping of a fluorescent ceramide analogue at the Golgi apparatus of fixed cells: interaction with endogenous lipids provides a trans-Golgi marker for both light and electron microscopy. *J Cell Biol* **109:** 2067–2079.

Pizarro-Cerda, J., Meresse, S., Parton, R.G., van der Goot, G., Sola-Landa, A., Lopez-Goni, I., *et al*. (1998) *Brucella abortus* transits through the autophagic pathway and replicates in the endoplasmic reticulum of nonprofessional phagocytes. *Infect Immun* **66:** 5711–5724.

Rejman Lipinski, A., Heymann, J., Meissner, C., Karlas, A., Brinkmann, V., Meyer, T.F., and Heuer, D. (2009) Rab6 and Rab11 regulate *Chlamydia trachomatis* development and golgin-84-dependent Golgi fragmentation. *PLoS Pathog* **5:** e1000615.

Rizzuto, R., Marchi, S., Bonora, M., Aguiari, P., Bononi, A., De Stefani, D., *et al*. (2009) Ca(2+) transfer from the ER to mitochondria: when, how and why. *Biochim Biophys Acta* **1787:** 1342–1351.

Robertson, D.K., Gu, L., Rowe, R.K., and Beatty, W.L. (2009) Inclusion biogenesis and reactivation of persistent *Chlamydia trachomatis* requires host cell sphingolipid biosynthesis. *PLoS Pathog* **5:** e1000664.

Robinson, M.D., McCarthy, D.J., and Smyth, G.K. (2010) edgeR: a Bioconductor package for differential expression analysis of digital gene expression data. *Bioinformatics* **26:** 139–140.

Rockey, D.D., Fischer, E.R., and Hackstadt, T. (1996) Temporal analysis of the developing *Chlamydia psittaci* inclusion by use of fluorescence and electron microscopy. *Infect Immun* **64:** 4269–4278.

Rockey, D.D., Grosenbach, D., Hruby, D.E., Peacock, M.G., Heinzen, R.A., and Hackstadt, T. (1997) *Chlamydia psittaci* IncA is phosphorylated by the host cell and is exposed on the cytoplasmic face of the developing inclusion. *Mol Microbiol* **24:** 217–228.

Rockey, D.D., Scidmore, M.A., Bannantine, J.P., and Brown, W.J. (2002) Proteins in the chlamydial inclusion membrane. *Microbes Infect* **4:** 333–340.

Romero-Brey, I., Merz, A., Chiramel, A., Lee, J.Y., Chlanda, P., Haselman, U., *et al*. (2012) Three-dimensional architecture and biogenesis of membrane structures associated with hepatitis C virus replication. *PLoS Pathog* **8:** e1003056.

Rosenwald, A.G., and Pagano, R.E. (1993) Intracellular transport of ceramide and its metabolites at the Golgi complex: insights from short-chain analogs. *Adv Lipid Res* **26:** 101–118.

Rzomp, K.A., Scholtes, L.D., Briggs, B.J., Whittaker, G.R., and Scidmore, M.A. (2003) Rab GTPases are recruited to chlamydial inclusions in both a species-dependent and species-independent manner. *Infect Immun* **71:** 5855–5870.

Saka, H.A., Thompson, J.W., Chen, Y.S., Kumar, Y., Dubois, L.G., Moseley, M.A., and Valdivia, R.H. (2011) Quantitative proteomics reveals metabolic and pathogenic properties of *Chlamydia trachomatis* developmental forms. *Mol Microbiol* **82:** 1185–1203.

Sandvig, K., and van Deurs, B. (2002) Transport of protein toxins into cells: pathways used by ricin, cholera toxin and Shiga toxin. *FEBS Lett* **529:** 49–53.

Sandvig, K., and van Deurs, B. (2005) Delivery into cells: lessons learned from plant and bacterial toxins. *Gene Ther* **12:** 865–872.

Schapiro, F.B., Lingwood, C., Furuya, W., and Grinstein, S. (1998) pH-independent retrograde targeting of glycolipids to the Golgi complex. *Am J Physiol* **274:** C319–C332.

Scidmore, M.A., and Hackstadt, T. (2001) Mammalian 14-3-3beta associates with the *Chlamydia trachomatis* inclusion membrane via its interaction with IncG. *Mol Microbiol* **39:** 1638–1650.

Scidmore, M.A., Fischer, E.R., and Hackstadt, T. (1996a) Sphingolipids and glycoproteins are differentially trafficked to the *Chlamydia trachomatis* inclusion. *J Cell Biol* **134:** 363–374.

Scidmore, M.A., Rockey, D.D., Fischer, E.R., Heinzen, R.A., and Hackstadt, T. (1996b) Vesicular interactions of the *Chlamydia trachomatis* inclusion are determined by chlamydial early protein synthesis rather than route of entry. *Infect Immun* **64:** 5366–5372.

Scidmore, M.A., Fischer, E.R., and Hackstadt, T. (2003) Restricted fusion of *Chlamydia trachomatis* vesicles with endocytic compartments during the initial stages of infection. *Infect Immun* **71:** 973–984.

Shibata, Y., Voeltz, G.K., and Rapoport, T.A. (2006) Rough sheets and smooth tubules. *Cell* **126:** 435–439.

Stechmann, B., Bai, S.K., Gobbo, E., Lopez, R., Merer, G., Pinchard, S., *et al*. (2010) Inhibition of retrograde transport protects mice from lethal ricin challenge. *Cell* **141:** 231–242.

Subbarayal, P., Karunakaran, K., Winkler, A.C., Rother, M.,

Gonzalez, E., Meyer, T.F., and Rudel, T. (2015) EphrinA2 receptor (EphA2) is an invasion and intracellular signaling receptor for *Chlamydia trachomatis*. *PLoS Pathog* **11:** e1004846.
Subtil, A., Collingro, A., and Horn, M. (2014) Tracing the primordial Chlamydiae: extinct parasites of plants? *Trends Plant Sci* **19:** 36–43.
Swanson, M.S., and Isberg, R.R. (1995) Association of *Legionella pneumophila* with the macrophage endoplasmic reticulum. *Infect Immun* **63:** 3609–3620.
Tilney, L.G., Harb, O.S., Connelly, P.S., Robinson, C.G., and Roy, C.R. (2001) How the parasitic bacterium *Legionella pneumophila* modifies its phagosome and transforms it into rough ER: implications for conversion of plasma membrane to the ER membrane. *J Cell Sci* **114:** 4637–4650.
Wang, J., Duncan, D., Shi, Z., and Zhang, B. (2013) WEB-based GEne SeT AnaLysis Toolkit (WebGestalt): update 2013. *Nucleic Acids Res* **41:** W77–W83.
Welsch, S., Miller, S., Romero-Brey, I., Merz, A., Bleck, C.K., Walther, P., *et al*. (2009) Composition and three-dimensional architecture of the dengue virus replication and assembly sites. *Cell Host Microbe* **5:** 365–375.
Wilfling, F., Thiam, A.R., Olarte, M.J., Wang, J., Beck, R., Gould, T.J., *et al*. (2014) Arf1/COPI machinery acts directly on lipid droplets and enables their connection to the ER for protein targeting. *Elife* **3:** e01607.
Wolf, K., and Hackstadt, T. (2001) Sphingomyelin trafficking in *Chlamydia pneumoniae*-infected cells. *Cell Microbiol* **3:** 145–152.
Wyrick, P.B., and Brownridge, E.A. (1978) Growth of *Chlamydia psittaci* in macrophages. *Infect Immun* **19:** 1054–1060.
Zhong, G., Fan, P., Ji, H., Dong, F., and Huang, Y. (2001) Identification of a chlamydial protease-like activity factor responsible for the degradation of host transcription factors. *J Exp Med* **193:** 935–942.

Supporting information

Additional supporting information may be found in the online version of this article at the publisher's web-site.